8-31-2002

Effects of Grand-Cycle Cessation on the Diagenesis of Upper Cambrian Carbonate Deposits in the Southern Appalachians, U.S.A

Bosiljka Glumac
Smith College, bglumac@smith.edu

Kenneth R. Walker
Smith College

EFFECTS OF GRAND-CYCLE CESSATION ON THE DIAGENESIS OF UPPER CAMBRIAN CARBONATE DEPOSITS IN THE SOUTHERN APPALACHIANS, U.S.A.

BOSILJKA GLUMAC[1] AND KENNETH R. WALKER[2]
[1] *Department of Geology, Smith College, Northampton, Massachusetts 01063, U.S.A.*
[2] *Department of Geological Sciences, The University of Tennessee, Knoxville, Tennessee 37996-1410, U.S.A.*
e-mail: bglumac@science.smith.edu

ABSTRACT: **The vertical transition from the mainly subtidal alternating shale and carbonate units (or grand cycles) of the Conasauga Group (Middle to Upper Cambrian) to the peritidal dolostone of the Knox Group (Upper Cambrian to Lower Ordovician) marks a major change in the early Paleozoic passive-margin sedimentation of the southern Appalachians. The grand cycles represent an interplay between intrashelf shale basin and carbonate-platform deposition. The end of grand-cycle deposition occurred in response to carbonate platform progradation over the infilled intrashelf basin and is associated with a prominent change in diagenetic patterns observed in the uppermost Conasauga Group strata—the Maynardville Formation. The Maynardville records upward shallowing from subtidal shale and limestone into peritidal dolostone. This change from a subtidal into a peritidal depositional regime influenced the early diagenesis of the Maynardville and, in conjunction with the changes in the regional facies distribution at the end of grand-cycle deposition, extended its influence upon the burial diagenesis of these deposits.**

The subtidal deposits of the Maynardville contain a variety of calcite cements. Dolomite is not abundant in these deposits, where it occurs mainly as a fine-crystalline ferroan phase associated with argillaceous layers and pressure-dissolution features. The local source for this dolomite during burial was provided by expulsion of pore fluids from interbedded shale deposits, diagenesis of clay minerals, and pressure dissolution of carbonates. Ferruginous coatings on hardgrounds in the subtidal deposits provided an additional local source of iron for the formation of replacement saddle dolomite. The subtidal deposits also contain saddle dolomite cement associated with Mississippi Valley–type (MVT) minerals, which indicate the involvement of externally derived fluids during late burial diagenesis of these strata. The peritidal deposits, on the other hand, are extensively dolomitized. Fine-crystalline dolomite most likely represents early diagenetic replacement of tidal-flat carbonate sediment. Coarse-crystalline replacement dolomite formed during burial by recrystallization of early dolomite and dolomitization by warm burial brines. Fenestrae, desiccation cracks, and evaporite-dissolution voids are occluded with dolomite cement, which is commonly complexly zoned. Zoned dolomite precipitated during shallow to intermediate burial and is postdated by saddle dolomite cement. Saddle dolomite in pore centers, dissolutional voids, and tectonic fractures formed during late burial from warm fluids associated with the migration of MVT brines.

The effects of changes in the depositional setting on diagenesis are reflected in similar early diagenesis between the subtidal Maynardville and the underlying Conasauga Group carbonate deposits, and between the peritidal deposits of the upper Maynardville and the rest of the overlying Knox Group. The depositional environments and early diagenesis also affected the burial diagenesis. The changes in regional facies distribution, caused by carbonate platform progradation at the end of grand-cycle deposition, resulted in a decrease in the proportion of siliciclastic components. This decrease was accompanied by a decline in the amount of ferroan carbonate in the peritidal deposits. The Maynardville is conformably overlain by carbonate deposits of the Knox Group. This allowed the Maynardville–Knox succession to behave as a single hydrologic unit for the migration of burial fluids in response to the formation of the Ordovician foreland (Sevier) basin to the southeast during the conversion from a passive into a convergent continental margin. The Nolichucky Shale separates the Maynardville–Knox succession from the carbonate deposits of the underlying Conasauga Group, which were, in contrast, affected by the migration of burial fluids from the Cambrian intrashelf shale basin to the west.

INTRODUCTION

The alternating shale and carbonate units of the Conasauga Group (Middle to Upper Cambrian) in the southern Appalachians (Fig. 1) are interpreted as grand cycles (Aitken 1981; Walker et al. 1990a; Srinivasan and Walker 1993; Rankey et al. 1994; Glumac and Walker 2000). These cycles represent third-order depositional sequences *sensu* Vail et al. (1977), and are also recognized in the Paleozoic sedimentary successions of the Great Basin, the Canadian Rocky Mountains, and the northern Appalachians (e.g., Mount and Rowland 1981; Chow and James 1987). The termination of grand-cycle deposition represents a prominent change in passive-margin sedimentation in the southern Appalachians. This change is reflected in the transition from the Conasauga Group into the overlying peritidal carbonate succession of the Knox Group (Upper Cambrian to Lower Ordovician; Fig. 1). The Maynardville Formation, which is the uppermost Conasauga Group, consists of a lower subtidal and an upper peritidal facies association (Fig. 1). The subtidal rocks consist of shale and limestone, which are similar to other Conasauga Group deposits. The peritidal deposits consist of extensively dolomitized rocks, which resemble the overlying Copper Ridge Dolomite and the rest of the Knox Group.

The distribution and characteristics of various diagenetic components from the Maynardville Formation and the lower part of the overlying Copper Ridge Dolomite were examined to document the relationship between the shift in the sedimentary regime and corresponding change in diagenetic patterns. This study focuses on the vertical transition from subtidal to peritidal deposition that resulted in the formation of distinct lithofacies, which differ in type and distribution of pores and occluding cement, and have undergone different styles of early diagenesis. Furthermore, the influence of the changes in the depositional environments and early diagenesis on late diagenesis is examined. The late diagenesis is considered in the context of changes in regional facies distribution and the burial history, which was controlled by the latest stages of passive-margin development and the transition into a convergent-margin setting.

GEOLOGIC SETTING OF THE STUDY AREA

The study area is within the Valley and Ridge physiographic province of northeastern Tennessee (Fig. 2). There, the Upper Cambrian strata dip to the southeast and crop out within several imbricated, northeast–southwest trending thrust blocks. Five stratigraphic sections from three thrust blocks were measured and sampled (Figs. 2, 3).

A passive continental margin was established along the eastern margin of North America following the breakup of the supercontinent Rodinia in the Late Precambrian and Early Cambrian (Bond et al. 1989). The sedimentary record of the southern Appalachians reveals the existence of a broad carbonate platform on this passive margin during the early Paleozoic (Fig. 2). The platform flanked the Iapetus Ocean to the east and the Conasauga intrashelf shale basin to the west (Fig. 2). In most of the eastern Tennessee Appalachians, Middle and Upper Cambrian sedimentation along the western margin of the carbonate platform produced alternating shale and carbonate units, or grand cycles, of the Conasauga Group (Figs. 1, 2). The grand cycles are replaced in northeasternmost Tennessee and southwestern Virginia by platform carbonate deposits (Honaker and Elbrook Dolomite), and towards the west by the Conasauga Shale. Carbonate deposition continued into the Early Ordovician, as evidenced by the shallow-water deposits (mainly dolostone) of the overlying Knox Group (Fig. 1). Passive-margin sedimentation terminated at the Lower Ordovician Knox–Beekmantown unconformity, which marks the transition into a convergent continental-margin setting (Shanmugam and Walker 1980; Read 1989).

METHODS

Petrographic analysis included examination of over 600 slabbed samples. Standard petrographic microscopy was carried out on 330 stained thin sections. Selected thin sections were examined using a Citl Cold Cathode Luminescence 8200 mk3 microscope under the following conditions: voltage 10–12 kV, beam current 150–180 μA, and chamber pressure 180–200 millitorr.

Samples for isotope analysis were collected by drilling 2–10 mg of individual carbonate components from polished thin-section billets using a microscope-mounted microdrill. Organic matter was removed by roasting the powdered samples at 380°C for one hour. Samples for oxygen and carbon isotope analysis were reacted off-line with 100% H_3PO_4 at 25°C for 24 hours (calcite) or 48 hours (dolomite). Analyses were made on a VG-903 isotope ratio mass spectrometer and are reported

JOURNAL OF SEDIMENTARY RESEARCH, VOL. 72, NO. 4, JULY, 2002, P. 570–586
 1527-1404/02/072-570/$03.00

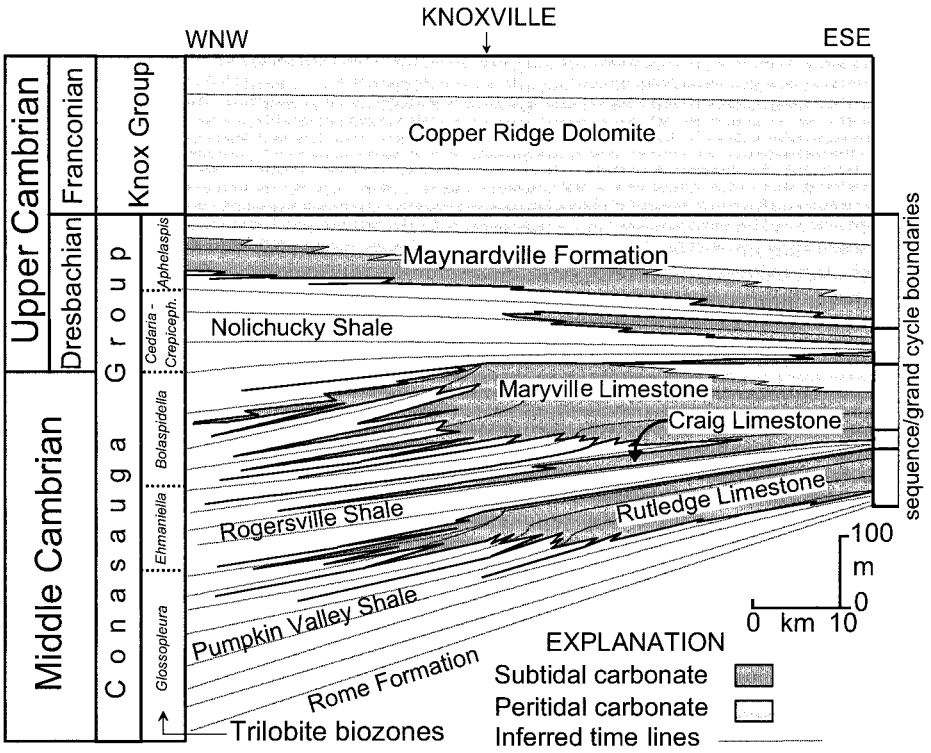

FIG. 1.—Middle to Upper Cambrian stratigraphy of eastern Tennessee Appalachians (modified from Walker et al. 1990a). Note interfingering relationship between shale and carbonate units (grand cycles) of the Conasauga Group, the predominance of carbonate in the Upper Cambrian (Maynardville–Copper Ridge), the distribution of subtidal and peritidal carbonate deposits, and the position of sequence (grand cycle) boundaries.

as $\delta^{13}C$ and $\delta^{18}O$ in permil (‰) relative to the PDB standard. External precision was $\pm$ 0.05‰ for both oxygen and carbon; sample reproducibility ($\pm$ 1σ) was 0.2‰.

Samples for radiogenic strontium isotope analyses were dissolved in 1.0 M Ultrex II acetic acid at room temperature. Prior to dissolution, samples were washed twice in 500 ml of 0.25 M Ultrex II acetic acid for 5 minutes, followed by two rinses with ultraclean Milli-Q deionized water to remove exchangeable Sr from clay minerals or other residue. Splits of powdered samples were also washed with 0.25 M ammonium acetate and leached in the same manner as above. The $^{87}Sr/^{86}Sr$ ratios of samples treated with ammonium acetate were compared with that of splits washed in dilute acetic acid to ensure that Sr was not derived from clays or other impurities. Sr isotope data were collected on a VG sector54 thermal ionization mass spectrometer in quintuple collector dynamic mode.

Major-element and trace-element compositions were analyzed on a Cameca SX-50 Electron Microprobe using polished thin sections, a defocused beam (10–20 μm in diameter), 25 kV accelerating voltage, and 10 nA beam current. Detection limits were 0.1 mole % $MgCO_3$ for Mg (count time = 20 s), 100 ppm for Mn and Fe, and 200 ppm for Sr (count time = 60 s). The calibration error was monitored by analyzing well-characterized carbonate standards.

PETROGRAPHIC CHARACTERIZATION

Vertical successions of various lithofacies comprising the subtidal and peritidal facies associations are illustrated in Figure 3. Detailed lithofacies descriptions and interpretations of depositional environments are included in Glumac (1997) and Glumac and Walker (2000). The following sections contain a summary of the charac-

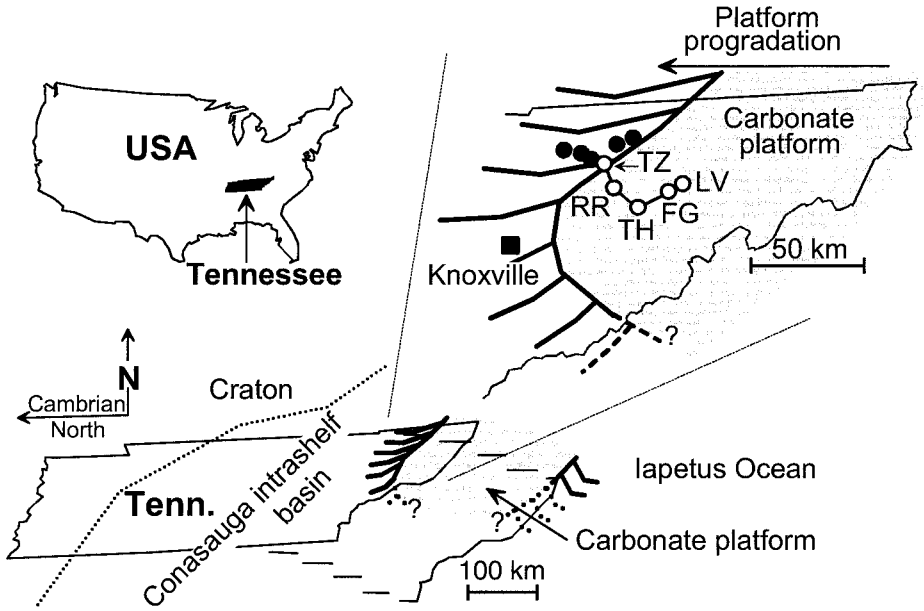

FIG. 2.—Schematic paleogeographic reconstruction of Tennessee during the Middle to early Late Cambrian (palinspastic reconstruction after Roeder and Witherspoon 1978). A dotted line shows the boundary between the exposed craton (to the west) and the Conasauga intrashelf basin (to the east). The area along the western carbonate platform margin is enlarged, showing present-day (solid circles) and palinspastically reconstructed (open circles) locations of the outcrops studied. Outcrop key: TZ, Tazewell; RR, River Ridge; TH, Thorn Hill; FG, Flat Gap; and LV, Lee Valley.

teristic petrographic observations with emphasis on the type and distribution of pores and the occluding cements. Various carbonate diagenetic components are illustrated in Figures 4–6 and described in greater detail in Table 1.

Subtidal Lithofacies

Ribbon rocks interbedded with shale, thrombolites, and ooid, skeletal, and intraclastic packstones and grainstones are the most common subtidal lithofacies (Fig. 3). The ribbon rocks consist of centimeter-scale alternating limestone and argillaceous layers. The matrix of the limestone layers is composed of a mosaic of aphanocrystalline to very fine-crystalline calcite, characterized by patchy distribution of bright to dull luminescence with many individual nonluminescent crystals. The subtidal micritic deposits are commonly burrow mottled. Burrows have diffuse walls, and are distinguished as patches of fine-crystalline ferroan calcite or microsparite and framboidal pyrite, which are also common adjacent to and within the argillaceous layers (Fig. 4A), and between allochems in skeletal packstones (Table 1A).

Interparticle pores in grainstone deposits are occluded with various types of calcite cements (Fig. 4B). Fibrous-to-bladed calcite is commonly the first generation of cement, and it shares compromise growth boundaries with syntaxial overgrowth calcite on echinoderm grains (Table 1A). Fine- to medium-crystalline equant calcite, here referred to as type 1 equant calcite cement, precipitated on fibrous-to-bladed calcite or as the first generation of cement in interparticle pores (Fig. 4B). Type 1 equant cement commonly has a drusy fabric, and it becomes less turbid in appearance and more ferroan in composition towards pore centers (Table 1A). Fibrous-to-bladed and type 1 equant calcite cements, similar to those from interparticle pores, also occlude burrows with sharp walls (borings) and framework voids in thrombolitic deposits (Fig. 4C). Centers of large interparticle voids and burrows are occluded with type 2 equant calcite cement, which consists of coarse-crystalline, nondrusy, turbid to clear crystals that commonly stain ferroan (Fig. 4D, E). Type 2 equant calcite is also present as the first generation of cement in voids of uncertain origin (dissolution-enlarged?), and is postdated by a dissolution event (Fig. 5A, B). Equant calcite crystals in these voids are characterized by clear, ferroan overgrowths on turbid, nonferroan cores (Fig. 5A). Dissolution-enlarged voids are common in the thrombolitic deposits and are mainly occluded with type 3 equant calcite cement (Fig. 4F) and rare saddle dolomite cement. Type 3 equant calcite forms a coarse-crystalline, nondrusy mosaic of clear, ferroan, uniformly non luminescent to dark dully luminescent crystals, which are also present in tectonic fractures (Table 1A).

Dolomite is not abundant in the subtidal deposits, and where present, it is ferroan. The most common type is fine-crystalline dolomite associated with the argillaceous layers of the ribbon rocks (Fig. 4A, B). Besides this dolomite, ferroan microsparite, and framboidal pyrite, the argillaceous layers also contain rare glauconite and numerous pressure-dissolution features (Fig. 4A). Coarse-crystalline saddle dolomite is present in the subtidal deposits as a later replacement phase, commonly associated with hardgrounds characterized by ferruginous crusts and coatings (Fig. 5C, D). Saddle dolomite is also present as a pore-central cement in dissolution-enlarged voids (Fig. 5A, B), and accompanied by rare Mississippi Valley–type (MVT) minerals such as galena, sphalerite, and pyrite in large interparticle pores in coarse-grained intraclastic deposits (Table 1B).

Peritidal Lithofacies

Peritidal lithofacies consist predominantly of mudstone and centimeter-scale, fining-upward couplets or mechanical laminites interbedded with a variety of microbial carbonate deposits, and less common ooid grainstone and calcareous siltstone (Fig. 3). These lithofacies are essentially devoid of skeletal remains (except for rare trilobite fragments associated with thrombolites and digitate stromatolites), and contain ample evidence for hypersaline conditions (evaporite pseudomorphs) and periodic subaerial exposure (mudcracks and scalloped erosional surfaces).

Most of the peritidal lithofacies are extensively dolomitized. Four dolomite replacement fabrics have been observed: dolomicrite, dolomicrosparite, coarse-crystalline dolomite (Fig. 6A), and saddle dolomite (Fig. 6B). Dolomicrite and dolomicrosparite are more abundant, finer-crystalline, have planar crystal boundaries, and are fabric retentive in comparison with the coarse-crystalline and saddle dolomite (Table 1B). The proportion of coarse-crystalline and saddle dolomite increases upsection.

Shallow subtidal thrombolites and digitate stromatolites are rare deposits in the peritidal facies association that have escaped complete dolomitization (Glumac and Walker 1997). These microbial deposits are present in the bases of some of the meter-scale shallowing-upward cycles recognized within the succession of peritidal lithofacies (Glumac and Walker 2000). The upper parts of these cycles are composed of extensively dolomitized intertidal to supratidal micritic deposits, and cycle tops are capped with subaerial exposure surfaces (Fig. 3).

The most common pore types in the peritidal deposits are desiccation cracks, evaporite-dissolution pores, and fenestrae. These pores are occluded by dolomite cement, which is in many cases zoned (Fig. 6C–F). Small voids are occluded by nonluminescent dolomite, which is petrographically similar to cores of complexly zoned dolomite crystals from larger pores. The number and thickness of individual zones of dolomite cement, recognized using cathodoluminescence (CL), vary substantially between pores (Fig. 6E, F). The centers of large pores are occluded with coarse-crystalline, mostly nonluminescent saddle dolomite, which also occludes dissolutional voids and tectonic fractures (Fig. 6G, H).

GEOCHEMISTRY

A summary of geochemical data for the carbonate components examined is given in Table 2. Stable-isotope values, elemental compositions, and strontium isotope ratios for the components analyzed are illustrated in Figures 7, 8, and 9.

Stable Isotopes

In comparison to the estimated stable-isotope composition of Cambrian marine calcite ($\delta^{18}O$ = —5‰; $\delta^{13}C = -0.5$‰ PDB; Lohmann and Walker 1989) and Upper Cambrian–Lower Ordovician marine calcite ($\delta^{18}O = -5$ to -3‰; $\delta^{13}C = -1$ to $+2$‰ PDB; Gao and Land 1991), all carbonate components analyzed are depleted in ^{18}O and are generally enriched in ^{13}C (Fig. 7). The measured $\delta^{13}C$ values of various depositional and diagenetic components define a wide range (from -0.6 to $+5$‰; Fig. 7). The $\delta^{18}O$ values of calcimicritic matrix of microbial subtidal deposits (average = -9.9‰) are in general more negative than the matrix of associated nonmicrobial deposits (average = -7.8‰; Fig. 7A). The $\delta^{18}O$ values of various calcite cements from the subtidal deposits overlap significantly, and range from about -13‰ for some of the type 3 equant calcite cements to about -7.5‰ for some of the fibrous-to-bladed calcite cements (Fig. 7B). The $\delta^{18}O$ compositions of cement and replacement saddle dolomite from the subtidal deposits (-9.9 to -8.1‰) are more negative than those of the fine-crystalline dolomite from argillaceous layers of ribbon rocks (-8.1 to -6.0‰; Fig. 7A, B).

The $\delta^{18}O$ compositions of the four types of replacement dolomite from the peritidal deposits also show substantial overlap (Fig. 7C). The succession of replacement fabric from dolomicrite to dolomicrosparite, coarse-crystalline dolomite, and saddle dolomite is characterized by slight depletion in average $\delta^{18}O$ values (dolomicrite = -6.7‰; saddle dolomite = -7.7‰). Isotope values for the two types of dolomite cements from the peritidal deposits also overlap, but the average $\delta^{18}O$ value of zoned dolomite (-7.7‰) is less negative than that of saddle dolomite (-8.2‰; Fig. 7D).

Major and Trace Elements

Data points illustrating the Sr versus $MgCO_3$ concentrations in various calcite components from the subtidal deposits define three compositional fields: (1) Sr $\geq$ 2000 ppm and $MgCO_3 < 1.2$ mole %; (2) Sr between 200 and 2000 ppm and $MgCO_3$ between 1 and 3 mole %; and 3) Sr $<$ 200 ppm, and $MgCO_3$ between 0.25 and 2.5 mole % (Fig. 8A). The first compositional field represents compositions of some of the fibrous-to-bladed calcite cement, whereas the second field comprises most of the remaining fibrous-to-bladed calcite, all micrite, and many of the type 1 equant calcite cements (Fig. 8A). The compositions of all remaining components (few fibrous-to-bladed calcite, many type 1 equant calcites, and all syntaxial and type 2 and 3 equant calcite cements) define the third compositional field, with the exception of a single type 3 equant calcite whose Sr composition reaches 340 ppm (Fig. 8A). The Fe and Mn concentrations of calcite components from the subtidal deposits have a significant intersample variation for most components, and range from below detection limit ($<$ 100 ppm) for some of the fibrous-to-bladed calcite and type 1 equant calcite cements to a maximum of 3181 ppm (micrite) and 531 ppm (fibrous-to-bladed calcite), respectively (Fig. 8B).

Saddle dolomite from the subtidal deposits has a nonstoichiometric composition, with the $CaCO_3$ content ranging from 53.2 to 55.5 mole % (Fig. 8C). Saddle dolomite cement has a somewhat higher $MgCO_3$ composition (average 42.4 mole %),

→

FIG. 3.—Stratigraphic columns of the Maynardville Formation and the lower Copper Ridge Dolomite. The columns are hung on the Maynardville–Copper Ridge boundary. Key to distance between outcrops: present day/palinspastically reconstructed distance. Outcrop key: TZ, Tazewell; RR, River Ridge; TH, Thorn Hill; FG, Flat Gap; and LV, Lee Valley.

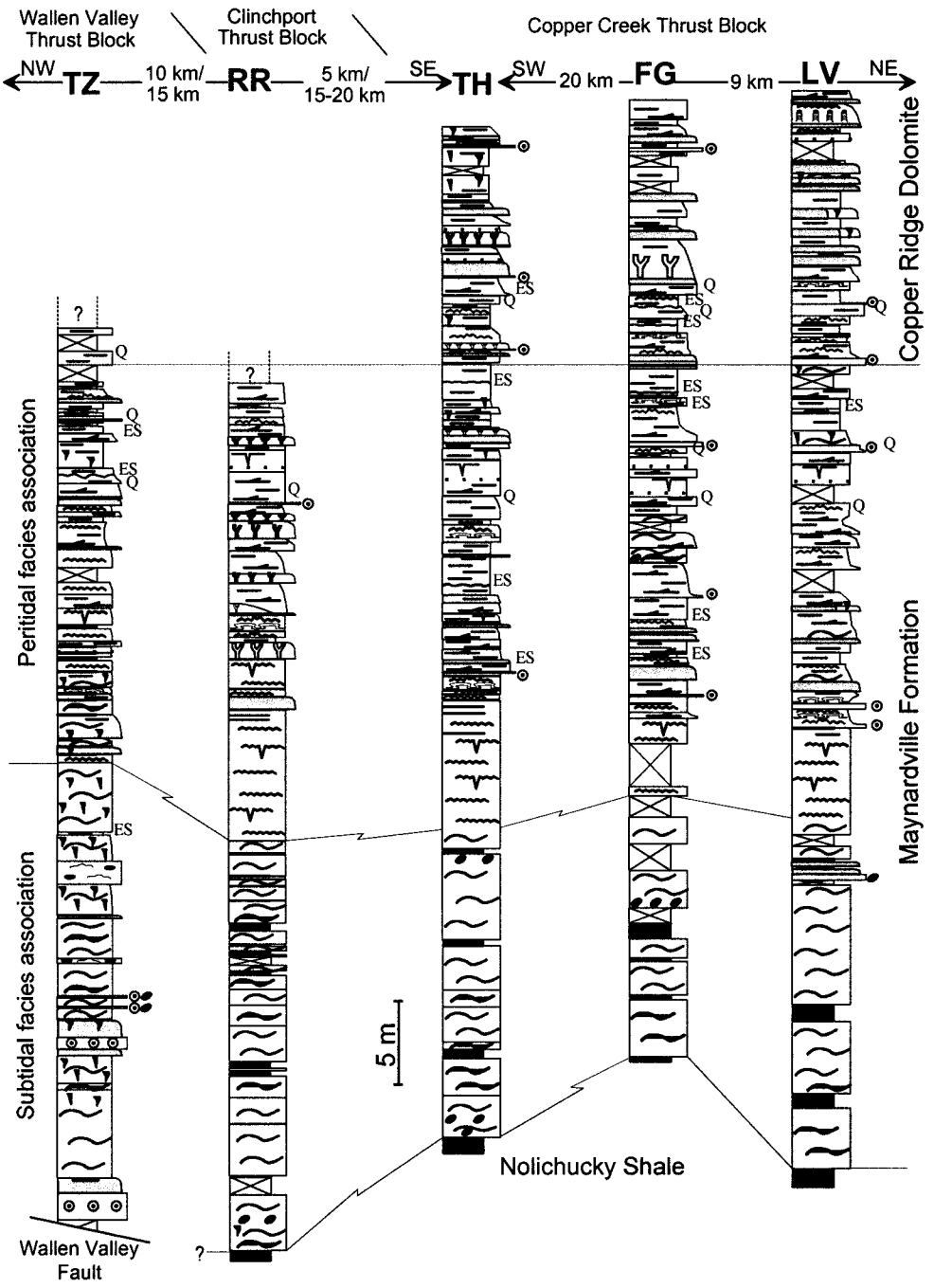

TABLE 1.—*Description of carbonate diagenetic components from the subtidal and peritidal lithofacies.*

	Occurrence	Description	Cathodoluminescence
A) subtidal lithofacies			
Calcite			
Microsparite	Associated with framboidal pyrite in burrows with diffuse walls in micritic layers of ribbon rocks. Adjacent to and within argillaceous layers of ribbon rocks. Replaces skeletal and micritic allochems and micritic matrix of packstone deposits.	Mosaic of very fine- to fine-crystalline (10–25 μm) calcite. Commonly stains ferroan.	Mainly non- to dark dull luminescent. Rare crystals are more brightly luminescent.
Fibrous-to-bladed calcite cement	First generation of cement. Fibrous morphology is commonly replaced by bladed (prismatic) crystals away from the substrate. Fibrous cement is common as isopachous rims on ooids and trilobite fragments. Fibrous-to-bladed calcite also lines walls of burrows and framework voids in thrombolitic deposits.	Radial- and radiaxial-fibrous (length : width $>$ 6:1), and bladed (prismatic) crystals (1:1 $<$ length : width $<$ 6:1); maximum width = 200 μm; maximum length = 500 μm. Cloudy or turbid (inclusion rich).	Uniform to patchy non- to dark dull luminescence. Some crystals have nonluminescent cores and dull to bright terminations with complex banding.
Syntaxial calcite cement	Syntaxial overgrowth on echinoderm fragments in packstone/grainstone deposits. Rare coarse crystals poikilotopically engulf other allochems and share compromise growth boundaries with fibrous-to-bladed calcite.	Coarse crystalline (up to 2.5 mm). Turbid (inclusion-rich), with clear outer crystal rims.	Dark dull luminescence. Occasional more brightly luminescent patches and thin outer crystal rims.
Type 1 equant calcite cement	Precipitated on fibrous-to-bladed calcite or as the first generation of cement in intergranular pores and burrows. Completely occludes centers of small pores.	A drusy fabric of equidimensional fine- to medium-crystalline (up to 100 μm) crystals, which commonly become clear and ferroan towards pore centers.	Uniformly dark dull luminescent.
Type 2 equant calcite cement	Precipitated on fibrous-to-bladed and/or type 1 equant calcite cement in central parts of large pores. Makes pore-rim cement in voids of uncertain origin (dissolution enlarged?). Postdated by a dissolution event.	Non-drusy mosaic of coarse (up to 1 mm) crystals. Mostly ferroan in composition, or forms clear overgrowths on turbid nonferroan cores.	Common non- to dark dully luminescent subzones or dark cores and thicker, bright orange/yellow outer parts with dull patches or subzones.
Type 3 equant calcite cement	Occludes dissolution-enlarged voids (common in thrombolitic microbial deposits) and tectonic fractures. Associated with rare dolomite cement.	Coarse- to very coarse-crystalline (up to 3 mm) equant, nondrusy, clear, ferroan crystals.	Nonluminescent or uniformly dark (dull orange) luminescent.
Dolomite			
Fine-crystalline dolomite	Associated with clay seams in argillaceous layers of ribbon rocks and with small-amplitude stylolites in other deposits. Scattered crystals replace micritic matrix and allochems. Commonly associated with ferroan microsparite and framboidal pyrite.	Ferroan; very fine- to fine-crystalline (10–50 μm); anhedral to subhedral. Rare medium-crystalline ($<$150 μm) rhombohedral (planar-e) crystals.	Nonluminescent. Rare rhombohedral crystals have uniform or zoned dull to bright luminescence.
Replacement saddle dolomite	Selectively replaces allochems (skeletal fragments, peloids). In interparticle pores of skeletal packstone/grainstone as a possible replacement of preexisting cement. Associated with hardgrounds with ferruginous crusts and coatings on allochems.	Ferroan, coarse- to very coarse-crystalline (250 μm–1.5 mm) dolomite with curved crystal boundaries and characteristic undulatory extinction.	Nonluminescent. Less common dark dull luminescent crystals.
Saddle dolomite cement	Pore-central cement; postdates type 2 equant calcite cement; preceded by a dissolutional event. Associated with pyrite, rare galena, and sphalerite in coarse-grained intraclastic layers, and with some type 3 equant calcite cement in dissolutional voids and fractures.	Ferroan, very coarse-crystalline (1–4 mm) dolomite with curved crystal boundaries and undulatory extinction. Some crystals are brownish in plane light.	Nonluminescent to very dark dull reddish/brown luminescent. Occasional thin bright red/orange luminescent zone.
B) peritidal lithofacies			
Replacement			
Dolomicrite	The primary component of mud-rich deposits including: dolomitized mudstone, fine-grained mechanical laminites or couplets, upper micritic parts of medium- to coarse-grained couplets, and stratiform and domal stromatolites.	Fabric-retentive mosaic of aphanocyrstalline to very fine-crystalline ($<$10–15 μm) anhedral to euhedral (planar-e) dolomite.	Uniform to patchy non- to dark dull orange luminescence.
Dolomicrosparite	Similar to dolomicrite. Common in lower portions of medium/coarse-grained couplets and in microbial deposits. Forms irregular patches that crosscut lithologic boundaries.	Fabric retentive mosaic of fine-crystalline (15–60 μm) subhedral (planar-s) to euhedral (planar-e) dolomite.	Patchy non- to bright orange luminescence.
Coarse-crystalline dolomite	Increases in abundance upsection. Laminae and allochem ghosts indicate replacement of domal and columnar stromatolites, and oolitic, intraclastic, and peloidal deposits. Also occurs in fabric-obliterative mosaics and in patches in rare limestone deposits.	Xenotopic mosaic of medium to coarse (60–300 μm) crystals with irregular and nonplanar boundaries. Some crystals have turbid cores and clear outer parts.	Non- to dark dull luminescent. Patchy dull luminescence is associated with allochem ghosts.
Saddle dolomite	Least abundant replacement phase; restricted to the uppermost Maynardville and the Copper Ridge Dolomite. Fabric obliterate, patchy, irregular distribution. In some cases replaces burrows, and is embedded in dark, argillaceous and bituminous matrix.	Coarse- to very coarse-crystalline (up to 1–2 mm). Well developed curved crystal faces. Some crystals have turbid centers and less turbid to clear outer parts.	Nonluminescent to dark dull brown luminescent. The surrounding bituminous matrix has dark blue luminescence.
Cement			
Zoned dolomite cement	Completely occludes smaller desiccation, evaporite-dissolution, fenestral, and rare intergranular and oomoldic voids. Pore-rim cement in larger voids. Individual rhombohedral crystals occur on rims of dissolution-enlarged voids in rare nondolomitized thrombolitic deposits.	Medium- to coarse-crystalline (200 μm–1 mm). Individual pore-rim rhombohedral crystals ($<$300 μm). common turbid cores and less turbid outer parts. Uniform to undulatory extinction.	Complexly zoned. Number and thickness of zones vary. Turbid cores are dull luminescent, followed by several bright to dull luminescent zones, and an outermost non- to dark dull luminescent zone.
Saddle dolomite cement	Precipitated on pore-rim zoned dolomite cement in larger desiccation and evaporite-dissolution voids as the last, pore-occluding cement. Completely occludes tectonic fractures, dissolution voids, and voids of uncertain origin in fabric-obliterated deposits. Associated with sphalerite in fractures and dissolution pores.	Very coarse-crystalline (1–3 mm). Well developed curved crystal faces and undulatory extinction. Some crystals are uniformly turbid or have turbid cores and less turbid rims.	Similar to outermost part of zoned dolomite cement: nonluminescent with some very faint, dark dull luminescent zones. Turbid crystals are uniformly dark dull luminescent.

and lower Fe concentration (average $\sim$ 17,500 ppm) than replacement saddle dolomite from the subtidal deposits (average = 41.1 mole % $MgCO_3$ and $\sim$ 24,000 ppm Fe; Fig. 8C, D). The peritidal replacement and cement dolomites have a stoichiometric to Ca-rich (maximum 56.7 mole % $CaCO_3$) composition (Fig. 8C). Relative to the subtidal dolomite, peritidal dolomites have generally higher $MgCO_3$ and lower Fe and Mn concentrations (Fig. 8C, D).

The distribution of trace elements was also examined along transects through pores in the peritidal deposits occluded with zoned and saddle dolomite cements (Fig. 8E, F). In both cements the Fe concentrations increase from the rims towards the pore centers. The maximum Fe concentrations in the outer nonluminescent parts of the zoned dolomite (about 5000 ppm) are comparable to the lowest Fe concentrations in the saddle dolomite cement along pore rims (Fig. 8E, F).

Strontium Isotopes

The $^{87}Sr/^{86}Sr$ ratios of the micrite (0.7092) and fibrous-to-bladed calcite (0.7091) from the subtidal deposits are within the estimated range for Late Cambrian seawater (0.7090 to 0.7093; Burke et al. 1982; Keto and Jacobsen 1987), whereas the saddle dolomite cement from the subtidal deposits has a slightly higher $^{87}Sr/^{86}Sr$ value (0.7096; Fig. 9). The dolomicrite from the peritidal strata is also enriched in ^{87}Sr

TABLE 2.—*Summary of geochemical data for the carbonate components from the subtidal and peritidal lithofacies.*

A) subtidal lithofacies

Component	$\delta^{18}O$‰ PDB Range	$\delta^{18}O$‰ PDB Avg (n)	$\delta^{13}C$ ‰ PDB Range	$\delta^{13}C$ ‰ PDB Avg (n)	$^{87}Sr/^{86}Sr$
Micrite (nonmicrobial)	−8.98 to −7.16	−7.82 (20)	0.49 to 4.09	2.40 (20)	—
Micrite (microbial)	−10.98 to −8.71	−9.88 (7)	1.53 to 3.68	2.89 (10)	0.70920
Fibrous-to-bladed calcite cement	−10.16 to −7.48	−8.92 (17)	2.31 to 4.89	3.48 (17)	0.70910
Type 1 equant calcite cement	−10.65 to −8.83	−9.53 (11)	1.24 to 4.72	2.76 (11)	—
Type 2 equant calcite cement	−11.00 to −9.07	−9.87 (8)	1.97 to 3.19	2.53 (8)	0.70889
Type 3 equant calcite cement	−12.92 to −9.38	−11.22 (10)	0.70 to 3.29	2.28 (10)	—
Fine-crystalline dolomite	−8.15 to −6.05	−7.07 (12)	2.83 to 4.99	3.71 (12)	—
Replacement saddle dolomite	—	−8.13 (1)	—	3.39 (1)	—
Saddle dolomite cement	−9.90 to −8.41	−8.94 (3)	3.44 to 3.97	3.65 (3)	0.70960

Component	$CaCO_3$ mole % Range	$CaCO_3$ mole % Avg	$MgCO_3$ mole % Range	$MgCO_3$ mole % Avg	Fe ppm Range	Fe ppm Avg*	Mn ppm Range	Mn ppm Avg*	Sr ppm Range	Sr ppm Avg*
Micrite (nonmicrobial)	96.85–98.23	97.55	1.63–2.50	2.22	335–3181	847	<100–169	57/154	200–673	463
Fibrous-to-bladed calcite cement	97.38–99.54	98.24	0.16–2.52	1.58	<100–1712	33/306	<100–531	40/213	<200–2695	11/1092
Syntaxial calcite cement (clear)	97.46–99.21	98.32	0.71–2.37	1.54	153–1039	698	<100–264	69/154	<200	—
Type 1 equant calcite cement	96.98–99.18	98.23	0.75–2.90	1.63	<100–1337	43/633	<100–403	43/233	<200–1874	47/730
Type 2 equant calcite cement	97.31–99.31	98.63	0.62–2.53	1.25	345–727	512	<100–275	43/174	<200	—
Type 3 equant calcite cement	97.29–99.75	98.46	0.24–2.37	1.41	832–1748	1512	129–331	219	<200–340	96/340
Replacement saddle dolomite	53.83–55.28	54.74	39.59–42.22	41.10	20752–32663	23995	429–1057	653	<200	—
Saddle dolomite cement	53.23–55.57	54.53	40.95–43.91	42.36	12821–21962	17584	472–1100	847	<200	—

B) peritidal lithofacies

Component	$\delta^{18}O$ ‰ PDB Range	$\delta^{18}O$ ‰ PDB Avg (n)	$\delta^{13}C$ ‰ PDB Range	$\delta^{13}C$ ‰ PDB Avg (n)	$^{87}Sr/^{86}Sr$
Dolomicrite (nonmicrobial)	−7.88 to −5.86	−6.78 (41)	0.32 to 4.68	3.13 (41)	0.70970
Dolomicrite (microbial)	−7.77 to −6.21	−6.70 (11)	0.67 to 4.38	3.13 (11)	—
Dolomicrosparite	−8.07 to −6.14	−6.83 (15)	1.52 to 4.78	3.51 (15)	—
Coarse-crystalline replacement dolomite	−9.04 to −6.09	−7.42 (12)	0.62 to 3.52	2.34 (12)	—
Saddle dolomite replacement	−10.51 to −6.44	−7.75 (8)	2.64 to 4.32	3.22 (8)	—
Zoned dolomite cement	−8.46 to −6.87	−7.70 (11)	1.27 to 3.37	2.46 (11)	0.70865; 0.70874
Saddle dolomite cement	−9.80 to −6.88	−8.21 (18)	−0.61 to 4.39	2.81 (18)	0.70866; 0.70896

Component	$CaCO_3$ mole % Range	$CaCO_3$ mole % Avg	$MgCO_3$ mole % Range	$MgCO_3$ mole % Avg	Fe ppm Range	Fe ppm Avg*	Mn ppm Range	Mn ppm Avg*	Sr ppm Range	Sr ppm Avg*
Dolomicrite (nonmicrobial)	52.77–55.92	54.16	43.92–47.10	45.70	281–1315	774	<100–124	56/112	<200–288	78/254
Dolomicrite (microbial)	50.61–51.50	51.04	48.38–49.30	48.84	349–892	623	<100–157	78/154	<200	—
Coarse-crystall. replacement dol.	53.84–56.69	55.00	43.19–45.15	44.29	343–8214	4025	<100–431	27/274	<200	—
Saddle dolomite replacement	52.92–54.84	53.58	43.63–45.99	45.21	5426–9867	7025	<100–488	11/246	<200	—
Zoned dolomite cement	50.26–54.10	52.28	45.51–49.64	47.30	<100–4982	5/2471	<100–408	16/222	<200	—
Saddle dolomite cement	51.47–56.59	53.70	43.30–47.60	45.21	458–10670	6264	<100–618	11/339	<200–261	99/261

* For the set of data containing values below detection limits (100 ppm for Fe and Mn, and 200 ppm for Sr), the first number represents the percentage of analyses below detection limit, and the second number represents the average value for the analyses above the detection limit.

(0.7097) relative to estimated Late Cambrian seawater (Fig. 9). The $^{87}Sr/^{86}Sr$ compositions of all the other samples analyzed, including type 2 ferroan equant calcite (0.70889) and peritidal dolomite cements (0.70865 to 0.70896), are lower than the estimated range for Late Cambrian seawater and are, in fact, similar to Early and Middle Ordovician seawater composition (Fig. 9).

CARBONATE DIAGENESIS

This section highlights the major differences in diagenetic history between the carbonate deposits constituting the subtidal and peritidal facies associations (Fig. 3). Paragenetic sequences that illustrate these differences and their relation to the burial history of the strata in question are included in Figure 10. It is important to note that these strata were deposited during a large perturbation in the global cycling of carbon (Glumac and Walker 1998). A wide range in measured $\delta^{13}C$ values (−0.6 to + 5‰; Fig. 7) reflects a short-term secular increase in the carbon isotope ratio of Late Cambrian (Late Dresbachian to Early Franconian, or Steptoean) seawater by 4–5‰ and buffering of diagenetic carbonate components to the host-rock $\delta^{13}C$ values. Studies of coeval successions worldwide confirm the secular nature of this large positive carbon-isotope excursion (Brasier 1993; Saltzman et al. 1998; Saltzman et al. 2000). The $\delta^{13}C$ values of individual samples depend mainly on the stratigraphic position of the sample, which complicates a direct comparison of $\delta^{13}C$ values of various carbonate components (unless they are sampled from the same stratigraphic interval). Comparisons of isotope compositions between carbonate matrix and associated cements in stratigraphic context are discussed in greater detail in Glumac and Walker (1998).

Subtidal Lithofacies

Calcite.—The presence of hardgrounds and intraclasts (flat pebbles) in the ribbon rocks, and the formation of burrows with sharp walls (borings) and framework voids in thrombolites indicate that the lithification of carbonate mud was among the earliest events in the diagenetic history of the subtidal deposits. The $^{87}Sr/^{86}Sr$ value of micrite is similar to that of the fibrous-to-bladed calcite cement (Fig. 9) and is consistent with precipitation from Cambrian seawater (Fig. 10). The oxygen isotope composition of micrite and the fibrous-to-bladed calcite (about −11 to −7‰; Fig. 7A, B), however, is lower than that of estimated Cambrian marine calcite ($\delta^{18}O$ = −5 to −3‰; Lohmann and Walker 1989; Gao and Land 1991), indicating subsequent diagenetic modifications. Diagenetic alteration is additionally supported by the elemental compositions and the CL patterns of these components. A covariant trend between Mg and Sr concentrations is expected for marine calcite if these elements are derived directly from seawater (Carpenter et al. 1991; Major and Wilber 1991; Carpenter and Lohmann 1992; Frank and Lohmann 1996). The lack of positive linear correlation between Sr and Mg concentrations in the fibrous-to-bladed calcite analyzed (Fig. 8A) suggests that precipitation of this cement was influenced by water–rock exchange through dissolution and precipitation reactions (Lohmann 1988; Banner and Hanson 1990; Saller and Moore 1991). If aragonite was originally present in the sediment but was subsequently completely dissolved, leaving no relict structures, recognition of calcite with an aragonitic precursor may still be possible by its high Sr content. The high calcite $Sr/MgCO_3$ ratio may reflect replacement of aragonite (with 8000–10000 ppm Sr) under closed or partially closed diagenetic conditions (Davies 1977; Brand and Veizer 1980; Mazzullo 1980; Wiggins 1986; Lohmann 1988). The elevated Sr (close to and above 2000 ppm) and relatively low

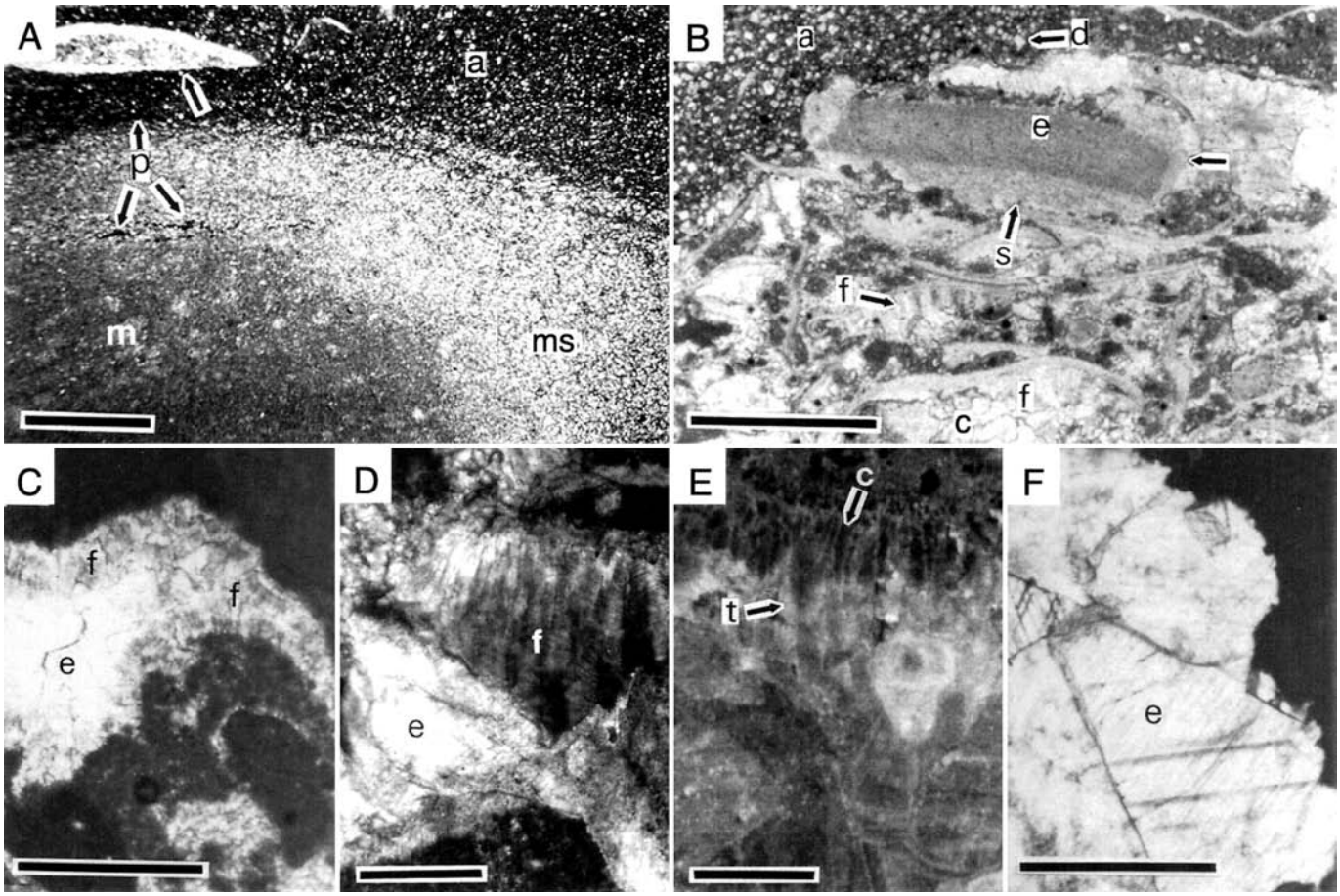

FIG. 4.—Photomicrographs of characteristic features of the subtidal deposits. **A)** Ribbon rock consisting of a dark-colored argillaceous layer above (a), and a limestone layer below. Partial dissolution of a skeletal fragment (trilobite) in the upper left corner is indicative of pressure dissolution (arrow). The limestone is composed of burrow-mottled micrite (m). Burrows and areas adjacent to the argillaceous layer are composed of ferroan microsparite (ms). Framboidal pyrite (p) is common in both limestone and argillaceous layers. Scale bar = 1 mm. **B)** Ribbon rock consisting of a skeletal packstone–grainstone layer adjacent to an argillaceous layer (a) with scattered dolomite crystals (d). Intergranular space is occluded with: syntaxial calcite cement overgrowth (s) on an echinoderm fragment (e), fibrous calcite (f) that precipitated on trilobite fragments in shelter voids, and some type 1 equant calcite cement (c). Arrow points to the boundary between an initial turbid and later clear syntaxial overgrowth cement. Scale bar = 1 mm. **C)** Framework void in thrombolite occluded by turbid fibrous-to-bladed calcite (f), and later pore-central type 1 equant calcite cement (e). Scale bar = 1 mm. **D)** Fibrous-to-bladed calcite cement (f), postdated by type 2 equant calcite (e) cement (cross-polars). **E)** On the paired CL photomicrograph fibrous-to-bladed calcite has nonluminescent cores (c) and more brightly luminescent crystal terminations (t). Equant calcite shows faint nonluminescent to dark dull luminescent zonation. Scale bar = 250 μm. **F)** Dissolution-enlarged void within thrombolite occluded with type 3 ferroan equant calcite cement (e). Scale bar = 1 mm.

$MgCO_3$ (< 1.2 mole %) content of the fibrous-to-bladed calcite (compositional field 1 in Fig. 8A), may thus suggest that precipitation of this cement was influenced by dissolution of precursor aragonite. No petrographic evidence for any relict aragonite fabrics or for a relationship between Sr concentration and calcite cement morphology and distribution was observed in the subtidal strata. Additionally, the high $Sr/MgCO_3$ ratio was documented for only a small portion of fibrous-to-bladed calcite crystals analyzed (compositional field 1 in Fig. 8A). In comparison, the micritic matrix has a relatively low Sr concentration (< 700 ppm) and a lower $Sr/MgCO_3$ ratio (compositional field 2 in Fig. 8A), which makes an aragonitic precursor unlikely (Wiggins 1986). A combination of these observations suggests that aragonite was not abundant in these Upper Cambrian subtidal deposits and that it may have been present exclusively as a marine cement whose wholesale dissolution in a locally closed diagenetic system preceded precipitation of the fibrous-to-bladed calcite cement with high Sr concentration.

The Sr and $MgCO_3$ compositions of the micritic matrix overlap with those of the fibrous-to-bladed calcite cement with elevated $MgCO_3$ (1 to 2.5 mole %) and lower Sr (< 2000 ppm) concentrations (compositional field 2 in Fig. 8A). The range of Sr concentrations in the components from this compositional field may reflect various degrees of diagenetic alteration, judging from the composition of modern marine Mg-calcites (900 to 1500 ppm Sr) and their diagenetically stabilized counterparts (tens or a few hundreds of ppm Sr; Veizer 1983; Carpenter et al. 1991; Major and Wilber 1991). The $MgCO_3$ composition of these fibrous-to-bladed calcites and micrites is comparable to documented retention of several mole % of $MgCO_3$ in high-Mg calcite (> 4 mole % $MgCO_3$), which have been altered to low-Mg calcite (Lohmann and Meyers 1977; Mazzullo et al. 1990). Rare microdolomite inclusions in these fibrous-to-bladed calcite crystals also indicate that these cements may represent diagenetically stabilized high-Mg calcites (Lohmann and Meyers 1977). The absence of common microdolomite may indicate: (1) efficient removal of Mg during diagenetic stabilization; and/or (2) a relatively low original $MgCO_3$ content typical of intermediate-Mg calcite (4 to 12 mole % $MgCO_3$). Patchy luminescence (Table 1A), and the maximum Fe and Mn concentrations of the fibrous-to-bladed calcite (1712 and 531 ppm, respectively) and micrite (3181 and 169 ppm, respectively) may also be the result of stabilization of Mg-calcite (under reducing conditions), with a subsequent loss of Mg (Major et al. 1988; Meyers 1989). The CL zonation observed in terminations of some of the fibrous-to-bladed calcite crystals (Fig. 4E) indicates that Fe and Mn were incorporated during precipitation of these zones from suboxic to anoxic pore waters (Sansone et al. 1990; Hendry 1993; Tobin et al. 1996). Therefore, the fibrous-to-bladed calcite cements from the subtidal deposits are interpreted to have started precipitating in the marine diagenetic realm, continued precipitating during shallow burial as the chemistry of pore waters changed from oxic to suboxic and anoxic (Fig. 10), and have subsequently been subjected to various degrees of later diagenetic (deeper burial) modifications. The $\delta^{18}O$ values for the fibrous-to-bladed calcite and micrite support modifications in the presence of meteoric water and/or at elevated temperature during burial (Fig. 7A, B). During these diagenetic modifications the $\delta^{13}C$ values of the fibrous-to-bladed calcite was buffered to the carbon isotope composition of the host carbonate as determined by

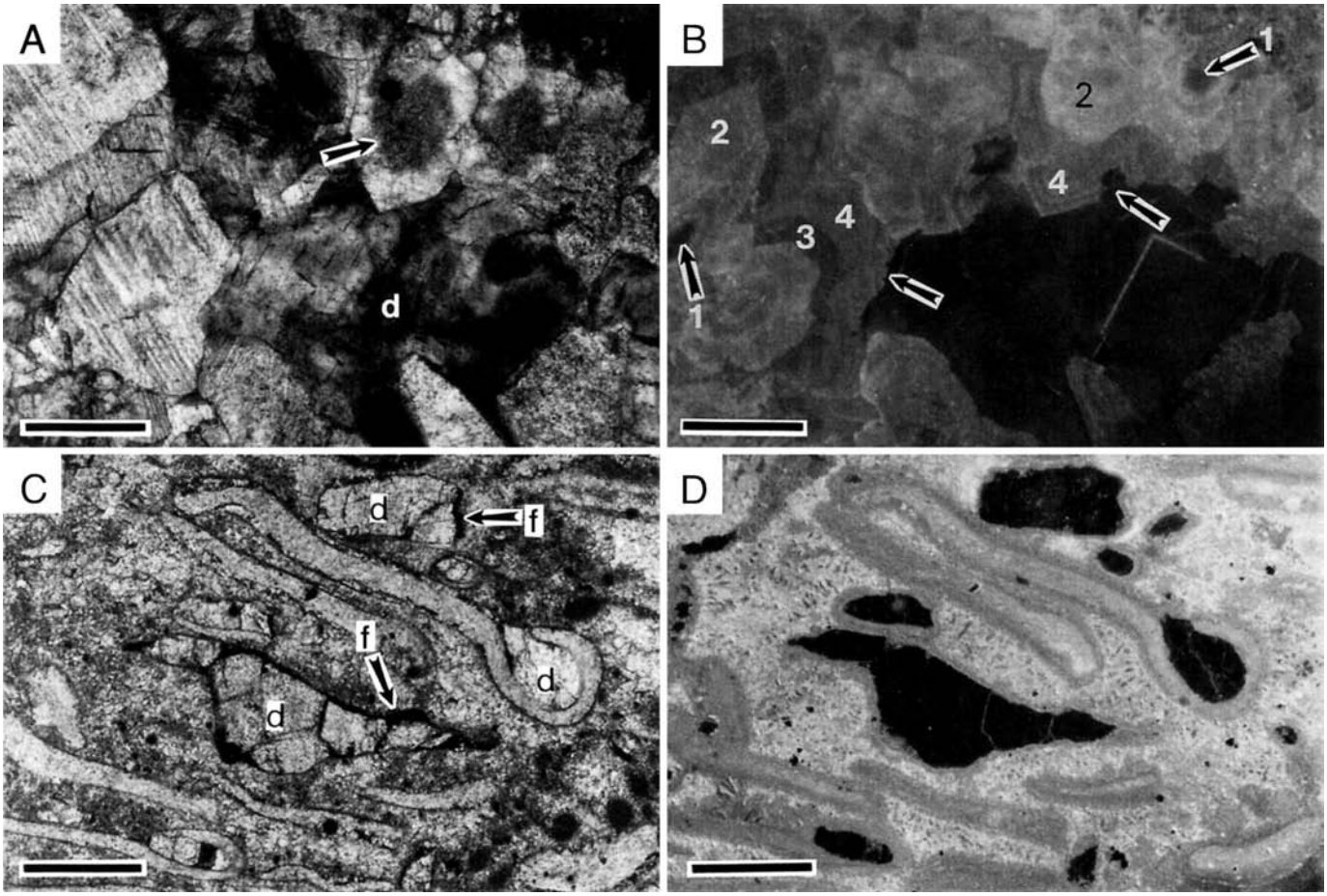

FIG. 5.—Paired plain-light and CL photomicrographs of equant calcite cement and saddle dolomite from the subtidal deposits. **A)** Saddle dolomite cement (d), surrounded by type 2 equant calcite cement. Arrow indicates a boundary between initial turbid and later clear calcite cements. **B)** Dolomite is nonluminescent on the paired CL photomicrograph, with the exception of one thin, brightly luminescent zone. Equant calcite cement is complexly zoned (zones 1–4). The boundary between zones 2 and 3 represents a transition from nonferroan to ferroan composition. The outer, ferroan zone of equant calcite was partially dissolved (arrows) prior to the precipitation of the saddle dolomite. Scale bar = 0.5 mm. **C)** Replacement saddle dolomite (d) in a skeletal packstone layer, about 1 cm below a hardground surface characterized by ferruginous coatings on allochems (f). **D)** Saddle dolomite is nonluminescent on the paired CL photomicrograph. Scale bar = 0.5 mm.

the comparison of the $\delta^{13}C$ values for associated carbonate matrix and cements in stratigraphic context (Glumac and Walker 1998). Pore fluids of meteoric origin may have affected subtidal deposits at shallow burial during repeated periods of subaerial exposure of the overlying peritidal deposits (Fig. 3). There is no petrographic evidence for extensive dissolution of subtidal deposits in the presence of meteoric fluids, even though the pores of uncertain origin, occluded with type 2 equant calcite cement, may be dissolution-enlarged pores (Fig. 5A, B). Extensive meteoric diagenesis may have been precluded by an arid to semiarid climate, short periods of subaerial exposure, paucity of aragonite, and the presence of calcite with relatively low Mg content (intermediate-Mg calcite).

The precipitation of calcite as syntaxial overgrowths on echinoderm fragments also likely started in the marine environment (Fig. 10). This is suggested by compromise growth boundaries with fibrous-to-bladed calcite (Table 1A), and the turbid appearance of the initial overgrowth cement (Fig. 4B), which is similar to the documented occurrences of inclusion-rich marine syntaxial cement (Hird and Tucker 1988; Walker et al. 1990b). Likewise, the precipitation of fine- to medium-crystalline equant calcite (type 1) as the first generation of cement in some intergranular pores and burrows (Table 1A) may have commenced from marine pore water (Fig. 10). Equant Mg-calcite can precipitate as a later phase in a succession of marine cement or in smaller pores with reduced fluid flow (Given and Wilkinson 1985; Gonzales et al. 1992). The trace-element composition of such equant calcite cements is commonly identical to that of associated marine calcite cements with elongated morphologies, which precipitated in larger pores with active circulation (Gonzales et al. 1992). Therefore, a similar diagenetic history is proposed for the type 1 equant calcite and fibrous-to-bladed calcite (see above) cements with overlapping Sr/$MgCO_3$ ratios (compositional field 2 in Fig. 8A) and Mn/Fe ratios (Fig. 8B). The stable-isotope compositions of these two types of cements overlap as well (Fig. 7B). The average $\delta^{18}O$ value for type 1 equant calcite (−9.5‰) is slightly lower than that for the fibrous-to-bladed calcite (−8.9‰), and this may indicate a possible precipitation of some of the type 1 equant cements from fluids of meteoric origin and/or at elevated temperature during burial (Fig. 10). The uncertainty in interpreting the origin of this cement reflects the fact that it is often difficult to distinguish between the products of meteoric phreatic and burial diagenesis (Tucker and Wright 1990; Saller and Moore 1991). Inclusion-free equant and syntaxial overgrowth calcite (Fig. 4B) are commonly interpreted as meteoric cements (James and Choquette 1984; Niemann and Read 1988; but see also Frank et al. 1995). Thus, the type 1 equant calcite cements with low Sr content (< 200 ppm), and whose composition overlaps with that of the clear syntaxial overgrowth calcite (compositional field 3 in Fig. 8A), are interpreted as shallow burial cements from pore fluids that may have been modified by mixing with meteoric water (Fig. 10).

Precipitation of type 2 equant calcite cement in voids that were likely dissolution enlarged, and the subsequent dissolution of this cement (Fig. 5A, B), suggest that the subtidal deposits experienced at least two separate dissolution events: (1) during shallow burial under the possible influence of meteoric fluids; and (2) deeper in the subsurface (Fig. 10). During the precipitation of the type 2 equant calcite cement on rims of dissolution-enlarged voids (Fig. 5A, B) and in centers of larger pores (Fig. 4D, E), pore-fluid chemistry fluctuated, as evidenced by the zonation observed in plane light and under CL. Characteristic features of this cement, such as the equant fabric, coarse crystallinity, and a decrease in the degree of turbidity, are all consistent with slower precipitation from fluids of lower saturation. Therefore, precipitation of type 2 equant cement (nonferroan cores) may have started during shallow burial from oxic waters of possible mixed marine–meteoric or meteoric origin,

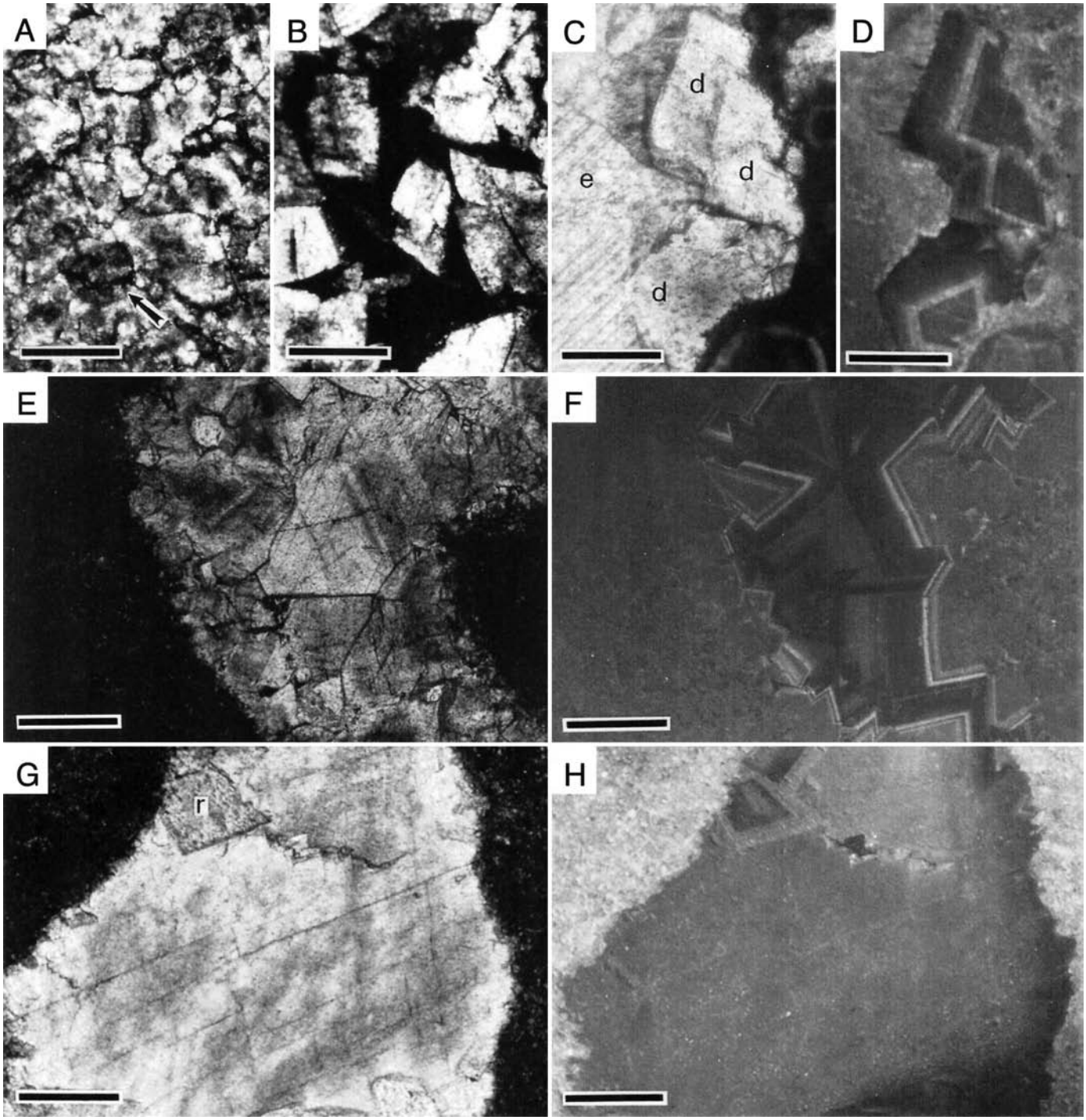

FIG. 6.—Photomicrographs of dolomite from the peritidal deposits. **A)** Xenotopic mosaic of coarse-crystalline replacement dolomite. Arrow points at an allochem ghost. Scale bar = 0.5 mm. **B)** Saddle dolomite in a dark bituminous matrix. Scale bar = 0.5 mm. **C)** Plain-light, and **D)** the paired CL photomicrograph of a zoned rhombohedral dolomite cement (d) postdated by type 3 ferroan equant calcite cement (e). Scale bar = 250 μm. **E)** Desiccation void occluded by dolomite cement showing a complex zonation on **F)** the paired CL photomicrograph. Scale bar = 0.5 mm. **G)** A void occluded by saddle dolomite cement and a rare pore-rim rhombohedral dolomite (r). **H)** On the paired CL photomicrograph rhombohedral dolomite is zoned, whereas saddle dolomite is uniformly nonluminescent to dark dull luminescent. Scale bar = 0.5 mm.

following the first dissolution event (Fig. 10), and continued as the conditions changed to suboxic and anoxic with progressive burial (ferroan zones; Fig. 5A, B). Precipitation from nonmarine or modified marine fluids is additionally supported by the Sr isotope composition of type 2 equant calcite ($^{87}Sr/^{86}Sr = 0.70889$), which is different from the estimated range of compositions for Late Cambrian seawater (Fig. 9). Shallow (meteoric phreatic) to later burial origin for the type 2 equant calcite is also substantiated by its negative $\delta^{18}O$ values (−11 to −9.1‰). Precipitation of type 2 equant calcite may have been coeval with the formation of: (1) the latest type 1 equant calcite in centers of small voids; (2) the clear outer zones of syntaxial overgrowth calcite (Fig. 4B); and (3) ferroan microsparite (Fig. 10). This is supported by similar Sr and $MgCO_3$ compositions of these components (field 3 in Fig. 8A), and by the elevated Fe and Mn concentrations of the type 1 equant calcite

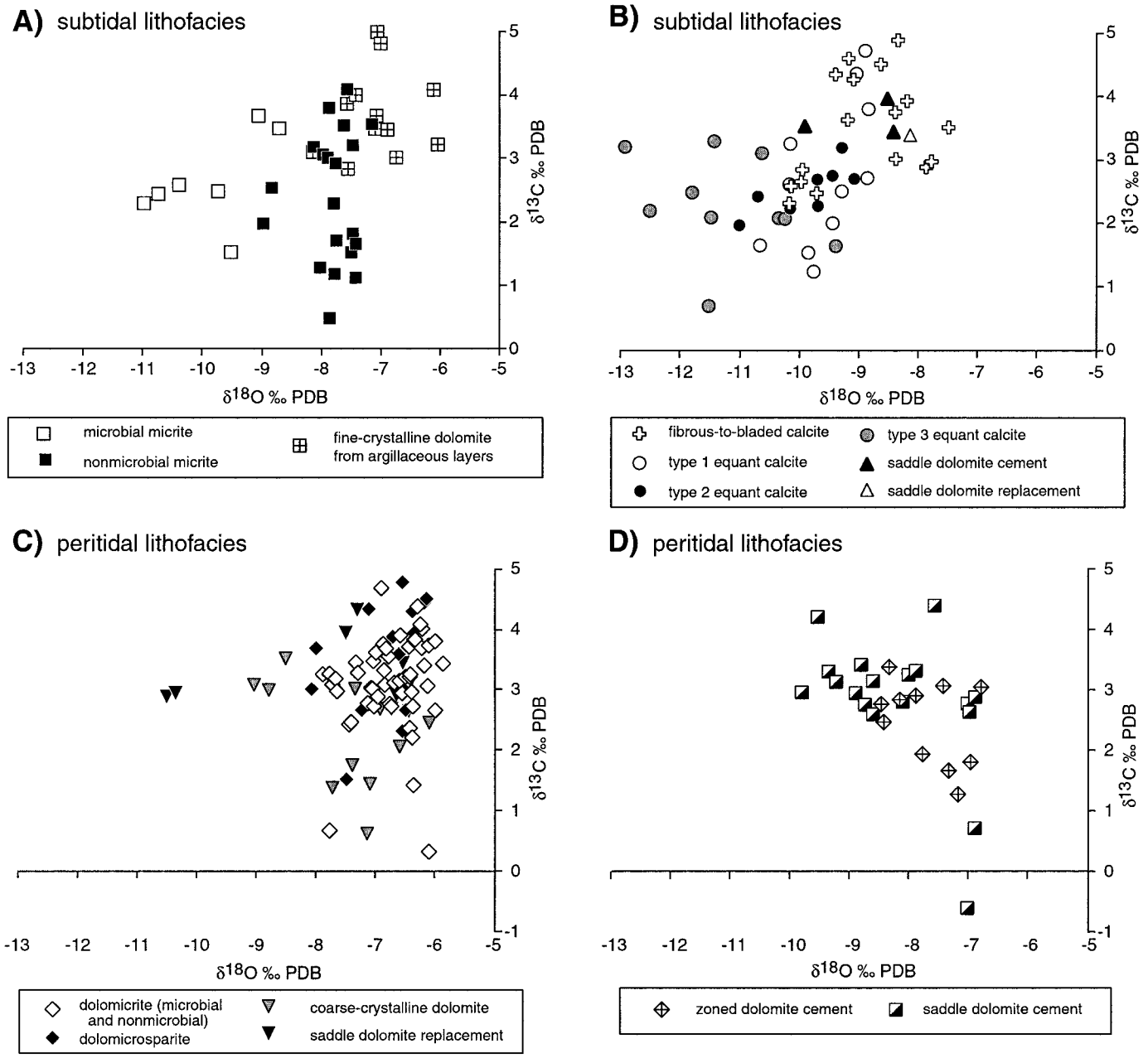

FIG. 7.—Stable-isotope compositions of various depositional and diagenetic components. Estimated composition of Cambrian marine calcite is: $\delta^{18}O = -5$ to -3‰ PDB; $\delta^{13}C = -1$ to $+2$‰ PDB (Lohmann and Walker 1989; Gao and Land 1991).

(maximum 1337 and 403 ppm, respectively), type 2 equant calcite (maximum 727 and 275 ppm, respectively), and syntaxial overgrowth calcite cements (maximum 1039 and 264 ppm, respectively; Fig. 8B).

Consistent with this interpretation are overlapping $\delta^{18}O$ values of the type 1 and type 2 equant calcite cements (Fig. 7B). The slightly more negative average $\delta^{18}O$ value of the type 2 equant calcite (−9.9‰) relative to type 1 equant calcite (−9.5‰) supports the interpretation that precipitation of coarse-crystalline type 2 equant calcite in larger pores continued during deeper burial, following the occlusion of small pores with type 1 equant calcite (Fig. 10). The $\delta^{13}C$ values of type 2 ferroan equant calcite cement from burrows in the subtidal deposits are commonly lower by 1 to 1.5‰ than those of the associated micritic matrix (Glumac and Walker 1998). This difference likely resulted from incorporation of ^{13}C-depleted carbon produced by organic-matter degradation processes, such as microbially mediated reduction reactions under suboxic conditions and/or subsequent abiogenic thermal decarboxylation processes under anoxic conditions at increased temperature during burial (Claypool and Kaplan 1974; Irwin et al. 1977; Coleman and Raiswell 1981; Winter and Knauth 1992). Glumac and Walker (1998) observed a wide scatter of $\delta^{13}C$ values, which is superimposed on the general stratigraphic trend of increasing carbon-isotope values in the subtidal micritic deposits of the lower Maynardville Formation. This trend marks the onset of the large positive Steptoean carbon-isotope excursion, and the scatter of $\delta^{13}C$ values is attributed to diagenesis of the subtidal deposits in the presence of degrading organic matter (Glumac and Walker 1998). This interpretation is substantiated by the association of ferroan carbonate phases (calcite cement and microsparite) with burrows, framboidal pyrite, fossiliferous lithofacies, and argillaceous layers of the subtidal deposits (Table 1A; Fig. 4A).

The presence of MVT minerals indicates the migration of externally derived burial brines through the subtidal deposits. A dissolution episode postdating precipitation of type 2 equant calcite cement (Figs. 5B, 10) indicates the presence of waters rich in organic acid or CO_2, which is a common characteristic of subsurface brines, including MVT mineralizing fluids (Meshri 1986; Spirakis and Heyl 1988; Mazzullo and Harris 1992; Gregg et al. 1993). The association of MVT minerals with the intraclastic deposits suggests preferential fluid migration through the coarse-grained

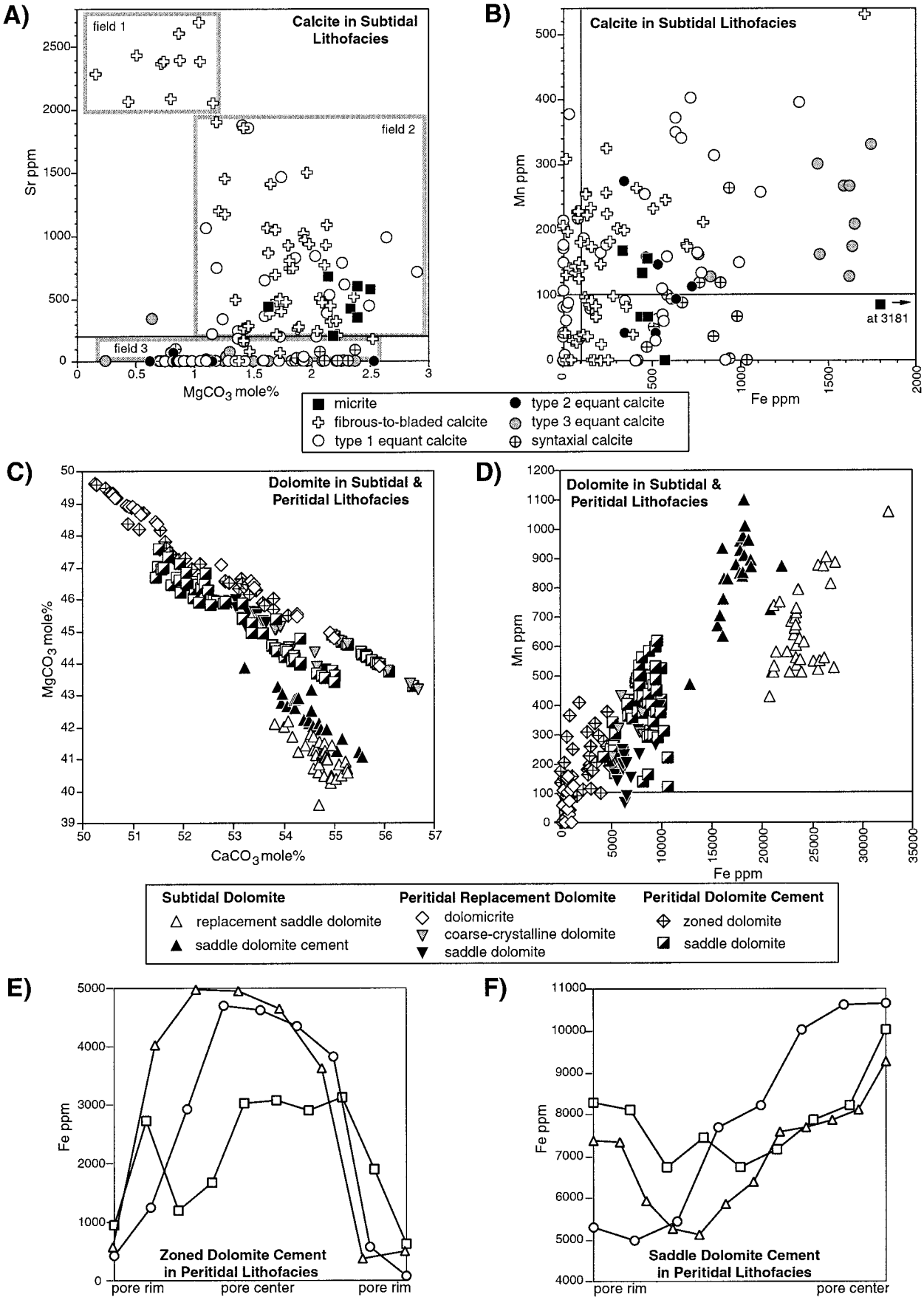

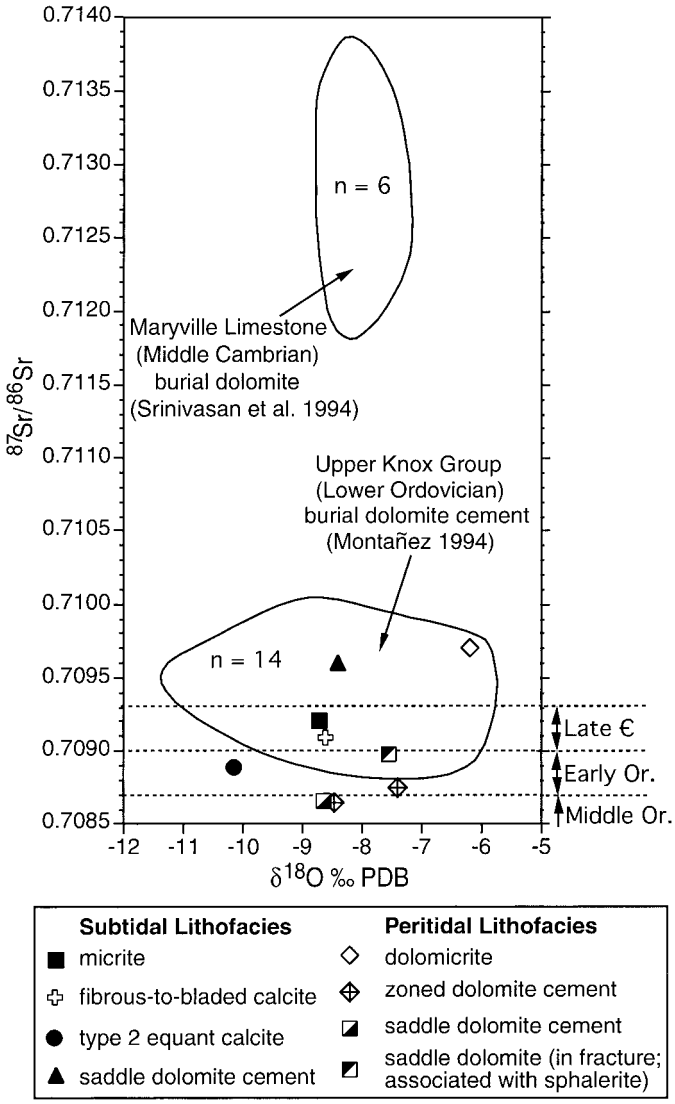

FIG. 9.—Sr isotope composition. Individual data points represent various components from the Upper Cambrian deposits. Compositional fields for burial dolomite from the Upper Knox (Montañez 1994) and the Maryville Limestone (Srinivasan et al. 1994) are shown for comparison. The Sr isotope composition for Ordovician and Late Cambrian seawater is indicated in the right margin (from Burke et al. 1982).

porous lithofacies (Table 1B). The framework pores and burrows in the microbial deposits, which had not been completely occluded during early diagenesis, may have also provided pathways for the migration of burial fluids, as suggested by common dissolution-enlarged pores in these deposits (Fig. 4F). Preferential movement of diagenetic fluids through porous microbial deposits may have resulted in more pronounced diagenetic alterations of these deposits, which is indicated by the more negative $\delta^{18}O$ values of microbial micrite (-11 to -8.7‰) in comparison with less porous nonmicrobial micrite (-9 to -7.2‰) from the subtidal deposits (Fig. 7A; Glumac 2001).

Most of the dissolution voids in the subtidal deposits are occluded with type 3 coarse-crystalline equant calcite (Fig. 4F) and pore-central saddle dolomite cements (Fig. 5A, B). These burial cements are also present in tectonic fractures (Table 1; Fig. 10). A burial origin for the type 3 equant calcite cements is supported by their $\delta^{18}O$ values (-12.9 to -9.4‰), which represent some of the most ^{18}O-depleted compositions in the suite of samples analyzed (Fig. 7B). Overlap in the $\delta^{18}O$ values of type 3 equant calcite with type 1 and 2 equant calcite and the fibrous-to-bladed calcite cements indicates modification of early diagenetic calcites during later diagenesis (Fig. 7B). The elevated Fe and Mn compositions (maximum 1748 and 331 ppm, respectively; Fig. 8B) and low $Sr/MgCO_3$ ratios (compositional field 3 in Fig. 8A) of type 3 equant calcite are also consistent with precipitation from burial fluids during late diagenesis. A single elevated Sr composition (340 ppm; Fig. 8A) most likely reflects buffering to the composition of the host rock and/or early diagenetic carbonate components.

Dolomite.—Formation of dolomite in the subtidal deposits did not require an abundant source of dolomitizing fluids because these deposits are not pervasively dolomitized. The $\delta^{18}O$ values of fine-crystalline dolomite in the argillaceous layers of the ribbon rocks (-8.2 to -6.1‰ PDB; Fig. 7A), which are lower than the -3 to $+1$‰ estimated range for dolomite precipitated in equilibrium with normal-salinity Late Cambrian seawater (based on the composition of Cambrian marine calcite and an equilibrium fractionation factor of 3 ± 1‰ between calcite and dolomite; Land 1985), suggests formation and/or alteration of this dolomite during burial. The association of fine-crystalline dolomite with pressure-dissolution features (Fig. 4A, B) suggests that this dolomite represents styloreactate minerals precipitated from fluids provided by dissolution of Mg-calcite and/or stylocumulates formed by concentrating dolomite as a less soluble residue. These interpretations are consistent with shallow to deeper burial formation of dolomite, prior to and during pressure dissolution of the subtidal deposits (Fig. 10). Dolomitizing fluids during shallow burial (prior to pressure dissolution) may have been at first provided by diffusion of overlying seawater and by dissolution of some of the host carbonate sediments (Mazzullo 2000; Teal et al. 2000), and by the subsequent compaction and expulsion of pore water from argillaceous sediment, with trapped seawater and ions adsorbed on clay-mineral surfaces serving as the source of Mg (Taylor and Sibley 1986; Coniglio and James 1988). Additional Mg ions may have been supplied by the release of structural water from clay minerals during illitization of smectite at temperatures > 50°C (Mattes and Mountjoy 1980; McHargue and Price 1982), which were reached within the first kilometer of burial of the subtidal deposits (Fig. 10). This process also produces Fe ions for the precipitation of dolomite enriched in Fe and accompanied by ferroan calcite (Taylor and Sibley 1986; Gregg 1988), and could explain the formation of the fine-crystalline ferroan dolomite associated with the ferroan microsparite in the subtidal deposits of the Maynardville Formation.

Burial dolomitization is also responsible for the formation of the saddle dolomite in the subtidal deposits (Fig. 10). The late burial origin for saddle dolomite is supported by its coarse-crystalline, nonplanar crystal morphology (Fig. 5), and by a nonstoichiometric (Ca-rich) composition and elevated Fe and Mn concentrations (Fig. 8C, D). Reduction or iron oxides and hydroxides from ferruginous crusts and coatings on hardgrounds provided an additional source of Fe for the replacement saddle dolomite (Fig. 5C). The $\delta^{18}O$ values of saddle dolomite (-9.9 to -8.1‰) are more negative than those of the fine-crystalline dolomite (-8.2 to -6.1‰; Fig. 7A, B) and indicate higher burial temperature and thus later burial for saddle dolomite (Fig. 10). The presence of MVT minerals (sphalerite, pyrite, galena) indicates the involvement of externally derived, warm basinal fluids in the diagenesis of the subtidal deposits (Table 1A). Precipitation of saddle dolomite cement was preceded by a dissolution event (Fig. 5A, B), which most likely took place during the initial encounter between the subtidal deposits and these subsurface brines (Fig. 10). Dissolution of carbonate host rock may have resulted in saturation of the brines and the subsequent precipitation of late diagenetic carbonate minerals. MVT mineralization by basinal brines is commonly associated with late burial dolomitization of carbonate deposits (Sverjensky 1981; Banner et al. 1988; among others). The Sr isotope composition of saddle dolomite cement in the subtidal deposits is elevated ($^{87}Sr/^{86}Sr = 0.7096$) relative to estimated Cambrian seawater (Fig. 9). This is consistent with precipitation of saddle dolomite from fluids that interacted with the interbedded subtidal argillaceous layers at elevated temperatures (Kesson et al. 1981; Stueber et al. 1987; Chaudhuri and Clauer 1992; Banner 1995). Temperatures be-

←

FIG. 8.—Elemental composition. **A)** $MgCO_3$ versus Sr composition of micrite and calcite cement from the subtidal deposits. Detection limit for Sr is shown as a horizontal line at 200 ppm. See text for explanation of compositional fields 1–3. **B)** Fe versus Mn composition of micrite and calcite cement from the subtidal deposits. Detection limit for both elements is 100 ppm. **C)** $CaCO_3$ versus $MgCO_3$ composition of subtidal and peritidal dolomite. **D)** Fe versus Mn composition of subtidal and peritidal dolomite. Detection limit for both Fe and Mn is 100 ppm. **E)** Fe compositional variations along transects through pores in the peritidal deposits occluded with the zoned dolomite cement. Transect lengths: 1.7 mm (circles), 2.7 mm (squares), and 1.8 mm (triangles). **F)** Fe compositional variations for saddle dolomite cement along transects from pore rim to pore center in the peritidal deposits. Transect lengths: 1.2 mm (circles), 0.9 mm (squares), and 1.6 mm (triangles).

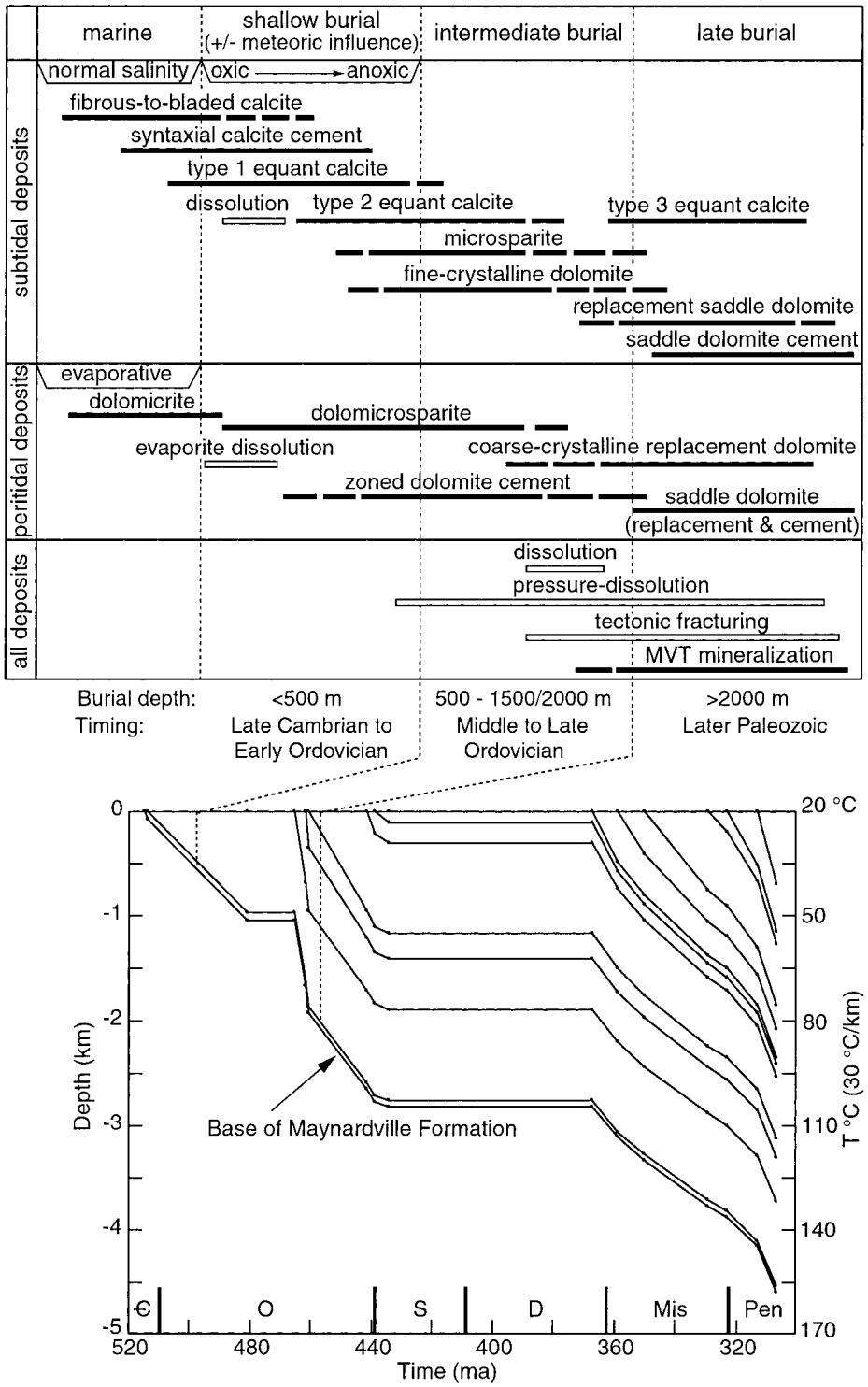

FIG. 10.—Paragenetic diagrams illustrating the relative timing of main events in the diagenetic history of the subtidal and the peritidal deposits, and the relationship with the burial history of these strata.

tween 90° and 175°C are suggested for precipitation of the saddle dolomite cement from the measured $\delta^{18}O$ values and an estimated range of possible $\delta^{18}O$ values for formation waters in sedimentary basins of 0 to 8‰ SMOW (Kharaka and Thordsen 1992; equations after Land 1985).

Peritidal Lithofacies

Replacement Dolomite.—Mechanisms and timing of massive dolomitization of ancient carbonate platform successions are still a matter of debate, but there is a consensus that most massive dolomites formed as replacement of metastable calcium carbonate and that a high concentration of Mg ions makes seawater an ideal source of dolomitizing fluids (McKenzie 1991). Features that suggest that dolomicrite from the peritidal deposits of the Maynardville Formation might be an early diagenetic replacement of muddy carbonate sediment on a semiarid tidal flat include: (1) a small crystal size and retention of the depositional fabric; (2) the association with intertidal to supratidal indicators such as evaporite molds, fenestrae, microbial laminae, desiccation features, and intraclasts; and (3) the paucity of fossils, indicating a restricted setting with elevated salinity in which penecontemporaneous dolomitization can sometimes be favored (Zenger and Dunham 1988). Additionally, an abun-

dant supply of Mg for pervasive dolomitization may have been provided by active circulation of seawater-derived fluids through the carbonate sediment during early diagenesis, prior to significant lithification and porosity occlusion. The argument for early diagenetic, syndepositional dolomitization from evaporation-modified seawater under sabkha-like conditions is strengthened by the occurrence of extensively dolomitized intertidal to supratidal deposits on top of rare nondolomitized shallow subtidal deposits in the bases of some of the meter-scale shallowing-upward cycles from the peritidal lithofacies succession (Fig. 3; Glumac and Walker 1997, 2000). Similar arguments (relative amount and stratigraphic position of dolomite within individual shallowing-upward cycles) were used in the interpretation of dolomicrite from the overlying Knox Group (Fig. 1; Montañez and Read 1992). In addition, the examined muddy subtidal and peritidal deposits have undergone a similar late (burial) diagenetic history, suggesting that the difference in conditions during deposition and early diagenesis of these deposits is most likely responsible for preferential dolomitization of the peritidal deposits (Fig. 10).

Early dolomite is very susceptible to alteration during subsequent diagenesis. The evidence for alteration of the early dolomite from the peritidal deposits includes: (1) the $\delta^{18}O$ values (-7.9 to $-5.9‰$; Fig. 7C), which reflect depletion in ^{18}O relative to dolomite precipitated in equilibrium with normal-salinity Late Cambrian seawater, and thus represent even greater depletion relative to dolomite precipitated from hypersaline fluids; and (2) the $^{87}Sr/^{86}Sr$ ratio, which is higher than estimated for Late Cambrian seawater (Fig. 9). A covariance between petrographic indicators, such as the neomorphic change from fine- to coarse-crystalline mosaics, and geochemistry (i.e., increased stoichiometry and decreased $\delta^{18}O$ values) is commonly used in identifying progressively altered dolomites (Sibley 1990; Gregg et al. 1992; Mazzullo 1992; Kupecz et al. 1993; Kupecz and Land 1994). Formation of coarse-crystalline dolomites may also occur as a replacement of limestone during late diagenesis in the deep subsurface (Machel and Anderson 1989; Mountjoy and Amthor 1994), and may be controlled by the coarse-grained texture of deposits being replaced (Sibley et al. 1993). It is commonly difficult to distinguish products of these processes from dolomites formed by neomorphism of early dolomite (Zenger and Dunham 1988). The following trends observed for the succession of replacement fabrics from: (1) dolomicrite; (2) dolomicrosparite; (3) coarse-crystalline dolomite; to (4) saddle dolomite in the peritidal deposits, suggest that this succession may represent the result of the progressive neomorphism of dolomite during burial: (1) an increase in crystal size; (2) an increase in the number of non-planar crystal boundaries; (3) an increase in fabric obliteration; (4) the slight decrease in average $\delta^{18}O$ values (from -6.7 to $-7.7‰$); and (5) with the exception of dolomicrosparite, which was not analyzed for trace-element composition, an increase in the average Fe concentration (from about 600 to 7000 ppm) and the maximum Mn concentration (from 124 to 488 ppm; Figs. 7C, 8D). This succession of replacement fabrics, however, is not accompanied by an apparent increase in stoichiometry (Fig. 8C), suggesting that other processes, instead of or in addition to neomorphism of early dolomite, may have been responsible for the formation of the coarse-crystalline dolomite from the peritidal deposits. A xenotopic fabric, the $\delta^{18}O$ values (-9 to $-6‰$), and an elevated trace element (up to 8200 ppm Fe and 430 ppm Mn) content of the coarse-crystalline replacement dolomite (Figs. 6A, 7C, 8D) support its formation by warm, deep subsurface fluids (Gregg and Sibley 1984; Zenger and Dunham 1988; Gregg et al. 1993). Any remaining limestone layers and grain-supported lithofacies may represent zones with higher porosity and permeability that serve as pathways for the preferential migration of such dolomitizing fluids during burial (Gao and Land 1991; Montañez and Read 1992; Kupecz et al. 1993; Mountjoy and Amthor 1994). The presence of allochem ghosts in the mosaic of coarse-crystalline dolomite (Fig. 6A) suggests replacement of coarse-grained (oolitic, intraclastic, and peloidal) deposits, whereas burial dolomitization of limestone is indicated by the patchy distribution of replacement dolomite within the rare limestone of the peritidal lithofacies succession (Table 1; Glumac and Walker 1997). In addition, the presence of saddle dolomite within a bituminous matrix in the peritidal deposits (Fig. 6B) suggests its formation related to hydrocarbon and basinal brine migration at elevated burial temperatures (60–150°C; Radke and Mathis 1980; Machel 1987). Thus, although it is almost certain that the fabric-obliterative mosaic of coarse-crystalline dolomite in the peritidal deposits formed during burial (Fig. 10), it is inconclusive whether it resulted from multiple recrystallization of early, fine-crystalline dolomite, and/or from burial replacement of limestone or grain-supported deposits.

Dolomite Cement.—The elemental concentrations and stable-isotope compositions of the zoned dolomite cement from the peritidal deposits overlap with those of the fine-crystalline replacement dolomite (Figs. 7C, D, 8C, D). This suggests that precipitation of the turbid, dully luminescent cores of these crystals, which fill or line pores of synsedimentary origin such as fenestrae and desiccation cracks (Table 2B; Fig. 6E, F), may have started during shallow burial simultaneously with early diagenetic alteration of dolomicrite in a rock-dominated system (Fig. 10). The low Fe content of the pore-rim zoned dolomite is also consistent with precipitation from oxygenated pore fluids during shallow burial (Fig. 8E).

There is no conclusive evidence that the precipitation of zoned dolomite cement was promoted by the introduction of meteoric water during repeated episodes of subaerial exposure of the peritidal deposits (Fig. 3). The possibility that this cement might represent mixed marine–meteoric dolomitization is suggested by the presence of zoned dolomite cements on walls of evaporite-dissolution voids, and by the similarity of this cement with documented occurrences of marine–meteoric mixing-zone, cavity-lining, rhombohedral dolomite crystals (1 to 100 μm), which are in places zoned and postdated by meteoric calcite (Fig. 6C, D; Kaldi and Gidman 1982; Ward and Halley 1985; Humphrey and Quinn 1989; Gill et al. 1995). The $\delta^{18}O$ values of zoned dolomite (-8.5 to $-6.9‰$) also do not offer a conclusive answer because they may reflect precipitation from fluids with a meteoric component or from burial fluids at elevated temperature (Fig. 7D). The lowest $\delta^{18}O$ values of zoned dolomite ($-8.5‰$) are more negative than the range of values for the dolomicrite (-7.9 to $-5.9‰$; Fig. 7C, D), and support the continuous precipitation of zoned dolomite during progressive burial (Fig. 10). Precipitation under reducing conditions during burial is additionally substantiated by the increased incorporation of Fe in the outer nonluminescent parts of the zoned dolomite cement (Fig. 8E), and by the maximum Fe and Mn concentrations (4982 and 408 ppm, respectively) in zoned dolomite in comparison to dolomicrite (maximum 1315 ppm Fe and 157 ppm Mn).

A source for the continuing precipitation of complexly zoned dolomite cement into the burial environment may have been provided by dissolution along numerous stylolites in the peritidal deposits and/or by externally derived basinal brines. Both of these processes have been used to explain precipitation of dolomite with complex zones that cannot be traced with certainty between pores (Fisher 1988; Amthor and Friedman 1992). The support for externally derived fluids (and against dissolution of Upper Cambrian marine carbonates) as the main source of dolomitizing fluid is provided by the Sr isotope compositions of the zoned dolomite cement from the peritidal deposits ($^{87}Sr/^{86}Sr = 0.70865$ and 0.70874), which are lower than the estimated range for Late Cambrian seawater (Fig. 9).

The zoned dolomite cement in larger desiccation and evaporite-dissolution voids is postdated by late diagenetic, nonluminescent to dark dull luminescent, coarse-crystalline saddle dolomite cement (Fig. 6G, H), which is also present as pore-rim cement in tectonic fractures and dissolution voids (Table 1B). The later burial origin for saddle dolomite cement is also supported by its elevated Fe and Mn concentrations (maximum 10670 and 618 ppm, respectively), and the more negative $\delta^{18}O$ values (-9.8 to $-6.9‰$) relative to the zoned dolomite cement (Figs. 7D, 8D–F). A combination of this petrographic and geochemical evidence, therefore, indicates mostly shallow to intermediate burial environments for the precipitation of zoned dolomite, and precipitation of the saddle dolomite cement during later, deep burial diagenesis (Fig. 10). The pore-central, nonluminescent to dark dully luminescent part of the zoned dolomite cement (Fig. 6F; Table 1B) may have precipitated simultaneously with saddle dolomite cement in larger pores (Fig. 10). This interpretation is supported by the overlap of $\delta^{18}O$ values of these two cement types (Fig. 7D), and their similar Sr isotope compositions (Fig. 9). The relatively low $^{87}Sr/^{86}Sr$ ratios of the saddle dolomite cement (0.70866 and 0.70896) are interpreted similarly to those of the zoned dolomite to indicate precipitation from an externally derived fluid with a source different from: (1) Late Cambrian seawater; (2) dissolution of Upper Cambrian carbonates; and (3) highly radiogenic basinal brines (Fig. 9). The association of saddle dolomite cement with sphalerite in fractures and dissolutional pores (Table 1B), suggests that these fluids most likely were MVT mineralizing brines. The saddle dolomite $\delta^{18}O$ values (-9.8 to $-6.9‰$; Fig. 7D) suggest a temperature of precipitation between 80° and 175°C (assuming $\delta^{18}O$ values of burial brines of 0 to 8‰ SMOW; Fig. 10). The $\delta^{18}O$ values of saddle dolomite are up to 2‰ lower than the dolomicritic matrix from the same stratigraphic interval, whereas its $\delta^{13}C$ values are identical to or less than 1‰ lower than associated dolomicrite (Glumac and Walker 1998). These observations are also consistent with formation of saddle dolomite during burial at elevated temperatures with $\delta^{13}C$ values being buffered to the host-rock composition.

DIAGENETIC HISTORY IN THE CONTEXT OF GRAND-CYCLE CESSATION

The changes in sedimentation patterns at the end of grand-cycle deposition in the southern Appalachians were controlled by the mechanisms related to the evolution of the early Paleozoic passive margin (Glumac and Walker 2000). These mechanisms include the stabilization of the margin in response to the cessation of episodic, nonthermal, tectonic subsidence, and the decrease in the thermal passive-margin subsidence rate. In conjunction with a long-term eustatic sea-level fall (Bond et al. 1989), these mechanisms favored the establishment of shallow-water carbonate deposition. As a consequence, during the Late Cambrian the carbonate platform prograded westward (cratonward) over the completely infilled Conasauga shale basin (Fig. 2). This resulted in the replacement of the subtidal shale and limestone of the Conasauga Group–lower Maynardville with peritidal carbonates of the upper May-

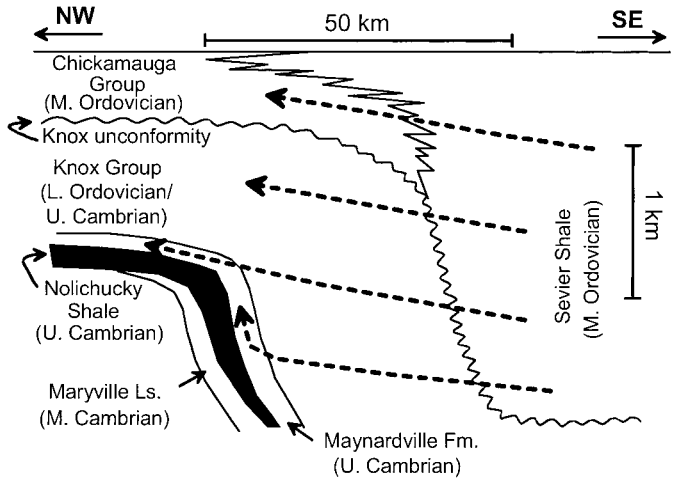

FIG. 11.—Schematic illustration of the compaction-driven fluid flow (dotted arrows) from the Sevier shale basin into the adjacent carbonate platform successions in eastern Tennessee (note vertical exaggeration). Stratigraphy from Walker (1980).

nardville–Knox Group (Figs. 1, 3). This study documents significant differences in the diagenesis of these deposits.

The early diagenesis of the subtidal deposits of the Maynardville Formation is similar to that of the Maryville Limestone (Middle Cambrian) of the Conasauga Group (Fig. 1; Srinivasan et al. 1994). Diagenesis of the subtidal Maynardville commenced in the presence of normal-salinity seawater (Fig. 10). Pore water of marine origin could have been modified by the introduction of meteoric water during a relative sea-level fall that converted subtidal depositional settings into extensive, periodically exposed tidal flats (Figs. 1, 3; Glumac and Walker 2000). On the other hand, the peritidal carbonate deposits of the upper Maynardville and the overlying Copper Ridge Dolomite experienced early diagenesis similar to that of the Upper Knox Group deposits (Montañez and Read 1992). The transition into peritidal deposition resulted in the pervasive, penecontemporaneous dolomitization of the tidal flat sediments. Differences in the depositional regime and early diagenesis also influenced the late diagenesis of the carbonate deposits of the terminal grand cycle. Argillaceous layers and hardgrounds with ferruginous crusts served as a local source of Fe for the formation of ferroan dolomite during burial of the subtidal deposits (Fig. 6C). The vertical decrease in the abundance of siliciclastic components in the Maynardville (Fig. 3) is coupled with a lower concentration of Fe in late diagenetic dolomite from the peritidal deposits (Fig. 8D), and with a lower abundance of ferroan carbonate phases in these deposits relative to the subtidal strata (Tables 1, 2).

The presence of MVT minerals confirms that burial diagenesis of these Upper Cambrian strata was influenced by the migration of externally derived warm basinal fluids (Fig. 10). The most probable source for the MVT brines in eastern Tennessee is the Middle Ordovician Sevier shale basin (Kesler et al. 1988; Kesler et al. 1989; Haynes and Kesler 1989). The Sevier Shale is made up of K-feldspar-poor volcanic detritus derived from a volcanic-arc source to the east and deposited in a subsiding foreland basin that developed in response to conversion of the region into a convergent continental margin (Fig. 11; Shanmugam and Walker 1980; Srinivasan et al. 1995). The establishment of this compressional tectonic regime, which lasted for the rest of the Paleozoic, was responsible for extensive deformation and fracturing of the lower Paleozoic strata in the area (Fig. 10).

The low Sr isotope ratios documented for the dolomite cement in the peritidal deposits (< 0.7087; Fig. 9) may reflect precipitation from Middle Ordovician marine pore waters with an original $^{87}Sr/^{86}Sr$ ratio between 0.7080 and 0.7087 (Burke et al. 1982; Keto and Jacobsen 1987), which were expelled from the Sevier Shale prior to substantial interaction with siliciclastic deposits (Fig. 11). Mechanical dewatering and the release of marine pore water from shale occur within the first 1 to 2 km of burial (Garven and Freeze 1984; Jones and Addis 1985). In eastern Tennessee, the Sevier Shale reaches a thickness of more than 2000 m, and its dewatering started as early as the Middle Ordovician (Fig. 11). This is in agreement with a proposed Middle Ordovician onset of MVT fluid migration in the southern Appalachians, and with these early brines representing connate waters expelled from the Sevier Shale (Kesler et al. 1989; Kesler and van der Pluijm 1990). The expelled pore water moved laterally into the Lower Ordovician Upper Knox carbonate strata (Fig. 11). The most extensive MVT mineralization is associated with the highly porous Upper Knox deposits, which were karstified and brecciated along the regional Knox unconformity (Fig. 11; Haynes and Kesler 1989; Montañez 1994). Montañez (1994) suggested that the dolomitizing fluids migrating through the Upper Knox deposits at intermediate depths (1.5–2.5 km) originated from burial-compaction dewatering of the Sevier Shale, whereas the late diagenetic (the Pennsylvanian–Early Permian) MVT fluids were meteoric waters that underwent interaction with the Sevier Shale during deep subsurface (2 to > 5 km) migration in response to Alleghenian tectonism and topography-driven recharge (Montañez 1994).

Such fluid migration through the Knox strata could have also influenced the underlying Maynardville deposits (Figs. 10, 11), as suggested by the increasing abundance of late diagenetic dolomite upsection. The late diagenetic dolomitization of the Upper Knox deposits was preceded by widespread dissolution (Montañez and Read 1992; Montañez 1994). The $^{87}Sr/^{86}Sr$ ratios of the dolomite cement from the Upper Cambrian peritidal deposits, which are within the proposed range for Early Ordovician seawater (0.7087 to 0.709; Fig. 9), may therefore indicate precipitation from burial fluids that interacted with the Lower Ordovician Knox carbonate rocks (Fig. 10). The Sr isotope composition of the Upper Knox (Lower Ordovician) burial dolomite cement examined by Montañez (1994) overlaps with or is more radiogenic than the dolomite cement in the Upper Cambrian peritidal deposits from this study (Fig. 9). This relationship may reflect evolution of basinal fluids resulting from the interaction with the Upper Knox carbonates as the fluids migrated into the Maynardville Formation (Fig. 11). The more radiogenic composition of the Knox burial dolomite (Fig. 9) also suggests that the substantial amount of porosity and permeability in the extensively karstified Upper Knox deposits allowed the migration of fluids that interacted with siliciclastics at higher temperatures during burial diagenesis, postdating the pore occlusion in the Maynardville Formation. This is additionally supported by the $\delta^{18}O$ values of the Knox burial dolomite (about -11 to -6‰; Montañez 1994), which reaches more negative values than the burial dolomite cement from the Maynardville deposits (Figs. 7D, 9).

The highly radiogenic Sr isotope composition of the late diagenetic dolomite from the Middle Cambrian Maryville Limestone of the Conasauga Group ($^{87}Sr/^{86}Sr = 0.7118$ to 0.7139; Figs. 1, 9), on the other hand, is interpreted to reflect the composition of fluids derived from the Cambrian Conasauga intrashelf shale basin located to the west of the carbonate platform (Fig. 2; Srinivasan et al. 1994; Srinivasan et al. 1995). K-feldspar- and mica-rich sediments in the Conasauga basin were derived from the weathering of cratonic crystalline basement rocks. Such sediments produce highly radiogenic formation waters (Stueber et al. 1987; McNutt et al. 1990; Banner 1995). The pronounced difference in the Sr isotope compositions between the burial dolomite in the Maryville and the Maynardville Formations (Fig. 9) suggests that the Maynardville deposits have not been significantly influenced by the migration of burial fluids from the Conasauga basin shale. Likewise, the burial fluids that migrated through the Upper Cambrian–Lower Ordovician carbonate succession did not significantly influence the Middle Cambrian carbonate deposits of the Conasauga Group (Fig. 11). The Nolichucky Shale (Upper Cambrian), which separates these two sedimentary successions, may have served as a barrier to cross-formational fluid migration (Figs. 1, 11). This illustrates yet another example of how a prominent change in the regional facies distribution, associated with the end of grand-cycle deposition, influenced burial diagenesis of Cambrian carbonate rocks in the southern Appalachians.

CONCLUSIONS

The Maynardville Formation, as a terminal-grand-cycle carbonate succession in the southern Appalachians, marks a prominent change in the deposition and diagenesis between the mainly subtidal Conasauga Group (Middle to Upper Cambrian) and the overlying Knox Group (Upper Cambrian to Lower Ordovician) peritidal carbonate deposits. The early diagenesis of the Maynardville was influenced by the change from a subtidal into a peritidal depositional regime. The subtidal deposits contain a variety of calcite cements of marine, possible meteoric, and burial origin. Most of the dolomite in the subtidal deposits is ferroan and fine-crystalline, and it formed during burial from fluids provided locally by compaction of argillaceous layers, pressure dissolution, and diagenesis of clay minerals.

The fine-crystalline dolomite in the peritidal deposits, on the other hand, is an early diagenetic replacement of tidal-flat carbonate sediment, and it was subsequently diagenetically modified. The coarse-crystalline replacement dolomite formed during burial by the recrystallization of early dolomite and/or dolomitization by warm basinal brines. The zoned dolomite cement in the peritidal deposits precipitated during shallow to intermediate burial, whereas the saddle dolomite cement formed during late burial from basinal brines related to MVT mineralization.

These basinal brines represent pore water expelled from the Middle Ordovician Sevier Shale, and fluids that interacted with Ordovician carbonate rocks. This is in marked contrast to the migration of basinal brines from the Conasauga Shale into the adjacent Middle Cambrian carbonate-platform strata. The differences in burial diagenesis of the Maynardville–Knox Group and the rest of the underlying Cona-

sauga Group carbonate deposits were influenced by changes in the regional facies distribution associated with the cessation of Cambrian grand-cycle deposition.

ACKNOWLEDGMENTS

This study was a part of the first author's dissertation research at the Department of Geological Sciences, The University of Tennessee, Knoxville (UTK). Partial support was provided by a Geological Society of America research grant and the UTK Faculty Senate Research Council Summer Research Assistantship to BG, and Discretionary and Mobil Carbonate Research Funds at the Department of Geological Sciences, UTK. Strontium isotope analyses were performed by S.A. Goldberg at the University of North Carolina at Chapel Hill. We are thankful to K.J. Tobin and A. Patchen for their help with electron microprobe analysis, and K. Howard and I. Richards for assistance with stable-isotope analysis. Discussions with C.I. Mora, K. Srinivasan, and other members of the Carbonate Research Group at UTK (1991–97) provided valuable insights. A.J. Caldanaro is thanked for help in the field and with illustrations. We are especially thankful for thoughtful reviews by S.J. Mazzullo, M.T. Harris, B. Kirkland-George, and M. Elrick.

REFERENCES

Aitken, J.D., 1981, Generalizations about Grand Cycles, *in* Taylor, M.E., ed., Short Papers for the Second International Symposium on the Cambrian System: U.S. Geological Survey, Open File Report 81–743, p. 8–14.

Amthor, J.E., and Friedman, G.M., 1992, Early- to late-diagenetic dolomitization of platform carbonates: Lower Ordovician Ellenburger Group, Permian Basin, West Texas: Journal of Sedimentary Petrology, v. 62, p. 131–144.

Banner, J.L., 1995, Application of the trace element and isotope geochemistry of strontium to studies of carbonate diagenesis: Sedimentology, v. 42, p. 805–824.

Banner, J.L., and Hanson, G.N., 1990, Calculation of simultaneous isotopic and trace element variations during water–rock interaction with applications to carbonate diagenesis: Geochimica et Cosmochimica Acta, v. 54, p. 3123–3127.

Banner, J.L., Hanson, G.N., and Meyers, W.J., 1988, Water–rock interaction history of regionally extensive dolomites of the Burlington–Keokuk Formation (Mississippian): Isotopic evidence, *in* Shukla, V., and Baker, P.B., eds., Sedimentology and Geochemistry of Dolostones: SEPM, Special Publication 43, p. 97–113.

Bond, G.C., Kominz, M.A., Steckler, M.S., and Grotzinger, J.P., 1989, Role of thermal subsidence, flexure, and eustasy in the evolution of early Paleozoic passive-margin carbonate platforms, *in* Crevello, P., Wilson, J.L., Sarg, J.F., and Read, J.F., eds., Controls on Carbonate Platform and Basin Development: SEPM, Special Publication 44, p. 39–61.

Brand, U., and Veizer, J., 1980, Chemical diagenesis of a multicomponent carbonate system—1: Trace elements: Journal of Sedimentary Petrology, v. 50, p. 1219–1236.

Brasier, M.D., 1993, Towards a carbon isotope stratigraphy of the Cambrian system: potential of the Great Basin succession, *in* Hailwood, E.A., and Kidd, R.B., eds., High Resolution Stratigraphy: Geological Society of London, Special Publication 70, p. 341–359.

Burke, W.H., Denison, R.E., Hetherington, E.A., Koepnick, R.B., Nelson, H.F., and Otto, J.B., 1982, Variation of seawater $^{87}Sr/^{86}Sr$ throughout Phanerozoic time: Geology, v. 10, p. 516–519.

Carpenter, S.J., and Lohmann, K.C., 1992, Sr/Mg ratios of modern marine calcite: empirical indicators of ocean chemistry and precipitation rate: Geochimica et Cosmochimica Acta, v. 56, p. 1837–1849.

Carpenter, S.J., Lohmann, K.C., Holden, P., Walter, L.M., Huston, T.J., and Halliday, A.N., 1991, $\delta^{18}O$ values, $^{87}Sr/^{86}Sr$ and Sr/Mg ratios of Late Devonian abiotic marine calcite: Implications for the composition of ancient seawater: Geochimica et Cosmochimica Acta, v. 55, p. 1991–2010.

Chaudhuri, S., and Clauer, N., 1992, Signatures of radiogenic isotopes in deep subsurface waters in continents, *in* Clauer, N., and Chaudhuri, S., eds., Isotopic Signatures and Sedimentary Records: New York, Springer-Verlag, p. 497–529.

Chow, N., and James, N.P., 1987, Cambrian Grand Cycles: A northern Appalachian perspective: Geological Society of America, Bulletin, v. 98, p. 418–429.

Claypool, G.E., and Kaplan, I.R., 1974, The origin and distribution of methane in marine sediments, *in* Kaplan, I.R., ed., Natural Gases in Marine Sediments: New York, Plenum Press, p. 99–140.

Coleman, M.L., and Raiswell, R., 1981, Carbon, oxygen and sulphur isotope variations in concretions from the Upper Lias of N.E. England: Geochimica et Cosmochimica Acta, v. 45, p. 329–340.

Coniglio, M., and James, N.P., 1988, Dolomitization of deep-water sediments, Cow Head Group (Cambro–Ordovician), western Newfoundland: Journal of Sedimentary Petrology, v. 58, p. 1032–1045.

Davies, G.R., 1977, Former magnesian calcite and aragonite submarine cements in upper Paleozoic reefs of the Canadian Arctic: A summary: Geology, v. 5, p. 11–15.

Fisher, H.J., 1988, Dolomite diagenesis in the Metaline Formation, northeastern Washington State, *in* Shukla, V., and Baker, P.B., eds., Sedimentology and Geochemistry of Dolostones: SEPM, Special Publication 43, p. 209–219.

Frank, T.D., and Lohmann, K.C., 1996, Diagenesis of fibrous magnesian calcite marine cement: Implications for the interpretation of $\delta^{18}O$ and $\delta^{13}C$ values of ancient equivalents: Geochimica et Cosmochimica Acta, v. 60, p. 2427–2436.

Frank, T.D., Lohmann, K.C., and Meyers, W.J., 1995, Chronostratigraphic significance of cathodoluminescence zoning in syntaxial cement: Mississippian Lake Valley Formation, New Mexico: Sedimentary Geology, v. 105, p, 29–50.

Gao, G., and Land, L.S., 1991, Geochemistry of Cambro–Ordovician Arbuckle limestone, Oklahoma: Implications for diagenetic $\delta^{18}O$ alteration and secular $\delta^{13}C$ and $^{87}Sr/^{86}Sr$ variation: Geochimica et Cosmochimica Acta, v. 55, p. 2911–2920.

Garven, G., and Freeze, R.A., 1984, Theoretical analysis of the role of groundwater flow in the genesis of stratabound ore deposits: 1. Mathematical and numerical model: American Journal of Science, v. 284, p. 1085–1124.

Gill, I.P., Moore, C.H., Jr., and Aharon, P., 1995, Evaporitic mixed-water dolomitization on St. Croix, U.S.V.I.: Journal of Sedimentary Research, v. A65, p. 591–604.

Given, R.K., and Wilkinson, B.H., 1985, Kinetic control of morphology, composition, and mineralogy of abiotic sedimentary carbonates: Journal of Sedimentary Petrology, v. 55, p. 109–119.

Glumac, B., 1997, Cessation of Grand Cycle Deposition in the Framework of Passive Margin Evolution: Controlling Mechanisms and Effects on Carbonate Deposition and Diagenesis, Cambrian Maynardville Formation, Southern Appalachians [unpublished Ph.D. thesis]: Knoxville, The University of Tennessee, 380 p.

Glumac, B., 2001, Influence of early lithification on late diagenesis of microbialites: Insights from $\delta^{18}O$ compositions of Upper Cambrian carbonate deposits from the southern Appalachians: Palaios, v. 16, p. 593–600.

Glumac, B., and Walker, K.R., 1997, Selective dolomitization of Cambrian microbial carbonate deposits: A key to mechanisms and environments of origin: Palaios, v. 12, p. 98–110.

Glumac, B., and Walker, K.R., 1998, A Late Cambrian positive carbon-isotope excursion in the southern Appalachians: relation to biostratigraphy, sequence stratigraphy, environments of deposition, and diagenesis: Journal of Sedimentary Research, v. 68, p. 1212–1222.

Glumac, B., and Walker, K.R., 2000, Carbonate deposition and sequence stratigraphy of the terminal Cambrian grand cycle in the southern Appalachians: Journal of Sedimentary Research, v. 70, p. 952–963.

Gonzales, L.A., Carpenter, S.J., and Lohmann, K.C., 1992, Inorganic calcite morphology: Roles of fluid chemistry and fluid flow: Journal of Sedimentary Petrology, v. 62, p. 382–399.

Gregg, J.M., 1988, Origins of dolomite in the offshore facies of the Bonneterre Formation (Cambrian), southeast Missouri, *in* Shukla, V., and Baker, P.B., eds., Sedimentology and Geochemistry of Dolostones: SEPM, Special Publication 43, p. 67–83.

Gregg, J.M., and Sibley, D.F., 1984, Epigenetic dolomitization and the origin of xenotopic dolomite texture: Journal of Sedimentary Petrology, v. 54, p. 908–931.

Gregg, J.M., Howard, S.A., and Mazzullo, S.J., 1992, Early diagenetic recrystallization of Holocene (< 3000 years old) peritidal dolomites, Ambergiris Bay, Belize: Sedimentology, v. 39, p. 143–160.

Gregg, J.M., Laudon, P.R., Woody, R.E., and Shelton, K.L., 1993, Porosity evolution of the Cambrian Bonneterre Dolomite, south-eastern Missouri, U.S.A.: Sedimentology, v. 40, p. 1153–1169.

Haynes, F.M., and Kesler, S.E., 1989, Pre-Alleghenian (Pennsylvanian–Permian) hydrocarbon emplacement along Ordovician Knox unconformity, eastern Tennessee: American Association of Petroleum Geologists, Bulletin, v. 73, p. 289–297.

Hendry, J.P., 1993, Calcite cementation during bacterial manganese, iron, and sulphate reduction in Jurassic shallow marine carbonates: Sedimentology, v. 40, p. 87–106.

Hird, K., and Tucker, M.E., 1988, Contrasting diagenesis of two carboniferous oolites from South Wales: a tale of climatic influence: Sedimentology, v. 35, p. 587–602.

Humphrey, J.D., and Quinn, T.M., 1989, Coastal mixing zone dolomite, forward modeling, and massive dolomitization of platform-margin carbonates: Journal of Sedimentary Petrology, v. 59, p. 438–454.

Irwin, H., Curtis, C., and Coleman, M., 1977, Isotopic evidence for source of diagenetic carbonates formed during burial of organic sediments: Nature, v. 269, p. 209–213.

James, N.P., and Choquette, P.W., 1984, Diagenesis 9. Limestones—The meteoric diagenetic environment: Geoscience Canada, v. 11, p. 161–194.

Jones, M.A., and Addis, M.A., 1985, Burial of argillaceous sediments: Marine and Petroleum Geology, v. 2, p. 247–253.

Kaldi, J., and Gidman, J., 1982, Early diagenetic dolomite cements: examples from the Permian lower magnesian limestone of England and the Pleistocene carbonates of the Bahamas: Journal of Sedimentary Petrology, v. 52, p. 1073–1085.

Kesler, S.E., Jones, L.M., and Ruiz, J., 1988, Strontium isotopic geochemistry of Mississippian Valley–type deposits, east Tennessee: implications for age and source of mineralizing brines: Geological Society of America, Bulletin, v. 100, p. 1300–1307.

Kesler, S.E., Gasink, J.A., and Haynes, F.M., 1989, Evolution of mineralizing brines in the east Tennessee Mississippi Valley–type ore field: Geology, v. 17, p. 466–469.

Kesler, S.E., and van der Pluijm, B.A., 1990, Timing of Mississippi-Valley–type mineralization: Relation to Appalachian orogenic events: Geology, v. 18, p. 1115–1118.

Kesson, K.M., Woddruff, M.S., and Grant, N.K., 1981, Gangue mineral $^{87}Sr/^{86}Sr$ ratios and the origin of Mississippi Valley–type mineralization: Economic Geology, v. 76, p. 913–920.

Keto, L.S., and Jacobsen, S.B., 1987, Nd and Sr isotopic variations of Early Paleozoic oceans: Earth and Planetary Science Letters, v. 84, p. 27–41.

Kharaka, Y.K., and Thordsen, J.J., 1992, Stable isotope geochemistry and origin of waters in sedimentary basins, *in* Clauer, N., and Chaudhuri, S., eds., Isotopic Signatures and Sedimentary Records: New York, Springer-Verlag, p. 411–466.

Kupecz, J.A., and Land, L.S., 1994, Progressive recrystallization and stabilization of early-stage dolomite, *in* Purser, B., Tucker, M., and Zenger, D., eds., Dolomites: A Volume in Honour of Dolomieu: International Association of Sedimentologists, Special Publication 21, p. 255–279.

Kupecz, J.A., Montañez, I.P., and Gao, G., 1993, Recrystallization of dolomite with time, *in* Rezak, R., and Lavoie, D.L., eds., Carbonate Microfabrics: New York, Springer-Verlag, Frontiers in Sedimentary Geology, p. 187–194.

LAND, L.S., 1985, The origin of massive dolomites: Journal of Geological Education, v. 33, p. 112–125.

LOHMANN, K.C., 1988, Geochemical patterns of meteoric diagenetic systems and their application to studies of paleokarst, *in* James, N.P., and Choquette, P.W., ed., Paleokarst: New York, Springer-Verlag, p. 58–80.

LOHMANN, K.C., AND MEYERS, W.J., 1977, Microdolomite inclusions in cloudy prismatic calcites: A proposed criterion for former high magnesium calcites: Journal of Sedimentary Petrology, v. 47, p. 1078–1088.

LOHMANN, K.C., AND WALKER, J.C.G., 1989, The $\delta^{18}O$ record of Phanerozoic abiotic marine calcite cements: Geophysical Research Letters, v. 16, p. 319–322.

MACHEL, H.G., 1987, Saddle dolomite as a by-product of chemical compaction and thermochemical sulfate reduction: Geology, v. 15, p. 936–940.

MACHEL, H.G., AND ANDERSON, J.H., 1989, Pervasive subsurface dolomitization of the Nisku Formation in Central Alberta: Journal of Sedimentary Petrology, v. 59, p. 891–911.

MAJOR, R.P., AND WILBER, R.J., 1991, Crystal habit, geochemistry, and cathodoluminescence of magnesian calcite marine cements from the lower slope of Little Bahama Bank: Geological Society of America, Bulletin, v. 103, p. 461–471.

MAJOR, R.P., HALLEY, R.B., AND LUKAS, K.J., 1988, Cathodoluminescent bimineralic ooids from the Pleistocene of the Florida continental shelf: Sedimentology, v. 35, p. 843–855.

MATTES, B.W., AND MOUNTJOY, E.W., 1980, Burial dolomitization of the Upper Devonian Miette Buildup, Jasper National Park, Alberta, *in* Zenger, D.H., Dunham, J.B., and Ethington, R.L., eds., Concepts and Models of Dolomitization: Society for Sedimentary Geology, Special Publication 28, p. 259–297.

MAZZULLO, S.J., 1980, Calcite pseudospar replacive of marine acicular aragonite, and implications for aragonite cement diagenesis: Journal of Sedimentary Petrology, v. 49, p. 409–422.

MAZZULLO, S.J., 1992, Geochemical and neomorphic alteration of dolomite: a review: Carbonates and Evaporites, v. 7, p. 21–37.

MAZZULLO, S.J., 2000, Organogenic dolomitization in peritidal to deep-sea sediments: Journal of Sedimentary Research, v. 70, p. 10–23.

MAZZULLO, S.J., AND HARRIS, P.M., 1992, Mesogenetic dissolution: Its role in porosity development in carbonate reservoirs: American Association of Petroleum Geologists, Bulletin, v. 76, p. 607–620.

MAZZULLO, S.J., BISCHOFF, W.D., AND LOBITZER, H., 1990, Diagenesis of radiaxial fibrous calcites in a subunconformity, shallow-burial setting: Upper Triassic and Liassic, Northern Calcareous Alps, Austria: Sedimentology, v. 37, p. 407–425.

MCHARGUE, T.R., AND PRICE, R.C., 1982, Dolomite from clay in argillaceous or shale-associated marine carbonates: Journal of Sedimentary Petrology, v. 52, p. 873–886.

MCNUTT, R.H., FRAPE, S.K., FRITZ, P., JONES, M.G., AND MACDONALD, I.M., 1990, The $^{87}Sr/^{86}Sr$ values of Canadian Shield brines and fracture minerals with applications to groundwater mixing, fracture history, and geochronology: Geochimica et Cosmochimica Acta, v. 54, p. 205–215.

MCKENZIE, J.A., 1991, The dolomite problem: An outstanding controversy, *in* Müller, D.W., McKenzie, J.A., and Weissert, H., eds., Controversies in Modern Geology: Evolution of Geological Theories in Sedimentology, Earth History and Tectonics: London, Academic Press, p. 37–54.

MESHRI, I.D., 1986, On the reactivity of carbonic and organic acids and generation of secondary porosity, *in* Gautier, D.L., ed., Roles of Organic Matter in Sediment Diagenesis: SEPM, Special Publication 38, p. 123–128.

MEYERS, W.J., 1989, Trace element and isotope geochemistry of zoned calcite cements, Lake Valley Formation (Mississippian, New Mexico): insights from water–rock interaction modelling: Sedimentary Geology, v. 63, p. 355–370.

MONTAÑEZ, I.P., 1994, Late diagenetic dolomitization of Lower Ordovician, Upper Knox carbonates: A record of the hydrodynamic evolution of the southern Appalachian Basin: American Association of Petroleum Geologists, Bulletin, v. 78, p. 1210–1239.

MONTAÑEZ, I.P., AND READ, J.F., 1992, Fluid–rock interaction history during stabilization of early dolomites, Upper Knox Group (Lower Ordovician), U.S. Appalachians: Journal of Sedimentary Petrology, v. 62, p. 753–778.

MOUNT, J.F., AND ROWLAND, S.M., 1981, Grand Cycle A (Lower Cambrian) of the southern Great Basin: A product of differential rates of relative sea-level rise, *in* Taylor, M.E., ed., Short Papers for the Second International Symposium on the Cambrian System: U.S. Geological Survey, Open-File Report 81–743, p. 143–146.

MOUNTJOY, E.W., AND AMTHOR, J.E., 1994, Has burial dolomitization come of age? Some answers from the western Canada Sedimentary Basin, *in* Purser, B., Tucker, M., and Zenger, D., eds., Dolomites: A Volume in Honour of Dolomieu: International Association of Sedimentologists, Special Publication 21, p. 203–229.

NIEMANN, J.C., AND READ, J.F., 1988, Regional cementation from unconformity-recharged aquifer and burial fluids, Mississippian Newman Limestone, Kentucky: Journal of Sedimentary Petrology, v. 58, p. 688–705.

RADKE, B.M., AND MATHIS, R.L., 1980, On the formation and occurrence of saddle dolomite: Journal of Sedimentary Petrology, v. 50, p. 1149–1168.

RANKEY, E.C., WALKER, K.R., AND SRINIVASAN, K., 1994, Gradual establishment of Iapetan ''passive'' margin sedimentation: stratigraphic consequences of Cambrian episodic tectonism and eustasy, southern Appalachians: Journal of Sedimentary Research, v. B64, p. 298–310.

READ, J.F., 1989, Controls on evolution of Cambro–Ordovician passive margin, U.S. Appalachians, *in* Crevello, P., Wilson, J.L., Sarg, J.F., and Read, J.F., eds., Controls on Carbonate Platform and Basin Development: SEPM, Special Publication 44, p. 147–165.

ROEDER, D., AND WITHERSPOON, W.D., 1978, Palinspastic map of east Tennessee: American Journal of Science, v. 278, p. 543–550.

SALLER, A.H., AND MOORE, C.H., 1991, Geochemistry of meteoric calcite cements in some Pleistocene limestones: Sedimentology, v. 38, p. 601–621.

SALTZMAN, M.R., RIPPERDAN, R.L., BRASIER, M.D., LOHMANN, K.C., ROBISON, R.A., CHANG, W.T., PENG, S., ERGALIEV, E.K., AND RUNNEGAR, B., 2000, A global carbon isotope excursion (SPICE) during the Late Cambrian: relation to trilobite extinctions, organic-matter burial and sea level: Palaeogeography, Palaeoclimatology, Palaeoecology, v. 162, p. 211–223.

SALTZMAN, M.R., RUNNEGAR, B., AND LOHMANN, K.C., 1998, Carbon isotope stratigraphy of Upper Cambrian (Steptoean Stage) sequences of the eastern Great Basin: Record of a global oceanographic event: Geological Society of America, Bulletin, v. 110, p. 285–297.

SANSONE, F.J., TRIBBLE, G.W., ANDREWS, C.C., AND CHANTON, J.P., 1990, Anaerobic diagenesis within Recent, Pleistocene, and Eocene marine carbonate frameworks: Sedimentology, v. 37, p. 997–1009.

SHANMUGAM, G., AND WALKER, K.R., 1980, Sedimentation, subsidence, and evolution of a foredeep basin in the Middle Ordovician, southern Appalachians: American Journal of Science, v. 280, p. 479–496.

SIBLEY, D.F., 1990, Unstable to stable transformation during dolomitization: Journal of Geology, v. 98, p. 739–748.

SIBLEY, D.F., GREGG, J.M., BROWN, R.G., AND LAUDON, P.R., 1993, Dolomite crystal size distribution, *in* Rezak, R., and Lavoie, D.L., eds., Carbonate Microfabrics: New York, Springer-Verlag, Frontiers in Sedimentary Geology, p. 195–204.

SPIRAKIS, C.S., AND HEYL, A.V., 1988, Possible effects of thermal degradation of organic matter on carbonate paragenesis and fluorite precipitation in Mississippi Valley–type deposits: Geology, v. 16, p. 1117–1120.

SRINIVASAN, K., AND WALKER, K.R., 1993, Sequence stratigraphy of an intrashelf basin carbonate ramp to rimmed platform transition: Maryville Limestone (Middle Cambrian), southern Appalachians: Geological Society of America, Bulletin, v. 105, p. 883–896.

SRINIVASAN, K., WALKER, K.R., AND GOLDBERG, S.A., 1994, Determining fluid source and possible pathways during burial dolomitization of Maryville Limestone (Cambrian), Southern Appalachians, U.S.A.: Sedimentology, v. 41, p. 293–308.

SRINIVASAN, K., WALKER, K.R., STEINHAUFF, D.M., GOLDBERG, S.A., AND RICIPUTI, L.R., 1995, Radiogenic Sr isotopes and rare earth elements as indicators of burial fluid sources in platform carbonates: Revisited (abstract): Geological Society of America, Annual Meeting, Abstracts with Programs, p. 273–274.

STUEBER, A.M., PUSHKAR, P., AND HETHERINGTON, E.A., 1987, A strontium isotopic study of formation waters from the Illinois Basin, U.S.A.: Applied Geochemistry, v. 2, p. 477–494.

SVERJENSKY, D.A., 1981, The origin of a Mississippi Valley–type deposit in the Viburnum Trend, southeast Missouri: Economic Geology, v. 76, p. 1848–1872.

TAYLOR, T.R., AND SIBLEY, D.F., 1986, Petrographic and geochemical characteristics of dolomite types and the origin of ferroan dolomite in the Trenton Formation, Ordovician, Michigan Basin: Sedimentology, v. 33, p. 61–86.

TEAL, C.S., MAZZULLO, S.J., AND BISCHOFF, W.D., 2000, Dolomitization of Holocene shallow-marine deposits mediated by sulfate reduction and methanogenesis in normal-salinity seawater, northern Belize: Journal of Sedimentary Research, v. 70, p. 649–663.

TOBIN, K.J., WALKER, K.R., SRINIVASAN, K., AND STEINHAUFF, D.M., 1996, Suboxic to anoxic diagenesis of platform-marginal ooids and bladed-to-fibrous calcite from the Middle Ordovician Ottosee Formation (east Tennessee): Geological Society of America, Bulletin, v. 108, p. 155–167.

TUCKER, M.E., AND WRIGHT, V.P., 1990, Carbonate Sedimentology: Boston, Blackwell Scientific, 482 p.

VAIL, P.R., MITCHUM, R.M., JR., AND THOMPSON, S., III, 1977, Seismic stratigraphy and global change of sea level, Part 4: Global cycles of relative changes of sea level, *in* Payton, C.E., ed., Seismic Stratigraphy—Applications to Hydrocarbon Exploration: American Association of Petroleum Geologists, Memoir 26, p. 83–97.

VEIZER, J., 1983, Trace elements and isotopes in sedimentary carbonates, *in* Reeder, R.J., ed., Carbonates: Mineralogy and Chemistry: Mineralogical Society of America, Reviews in Mineralogy, v. 11, p. 265–299.

WALKER, K.R., 1980, Introduction to the stratigraphy and paleoenvironments of the Middle Ordovician of Tennessee (southern Appalachians, U.S.A.), *in* Walker, K.R., Broadhead, T.W., and Keller, F.B., eds., Middle Ordovician Carbonate Shelf to Deep Water Basin Deposition in the Southern Appalachians: The University of Tennessee, Studies in Geology 4, p. 4–12.

WALKER, K.R., FOREMAN, J.L., AND SRINIVASAN, K., 1990a, The Cambrian Conasauga Group of Eastern Tennessee: A preliminary general stratigraphic model with a more detailed test for the Nolichucky Formation: Appalachian Basin Industrial Associates, v. 17, p. 184–189.

WALKER, K.R., JERNIGAN, D.G., AND WEBER, L.J., 1990b, Petrographic criteria for the recognition of marine, syntaxial overgrowths and their distribution in geologic time: Carbonates and Evaporites, v. 5, p. 141–152.

WARD, W.C., AND HALLEY, R.B., 1985, Dolomitization in a mixing zone of near-seawater composition, Late Pleistocene, northeastern Yucatan Peninsula: Journal of Sedimentary Petrology, v. 55, p. 407–420.

WIGGINS, W.D., 1986, Geochemical signatures in carbonate matrix and their relation to deposition and diagenesis, Pennsylvanian Marble Falls Limestone, Central Texas: Journal of Sedimentary Petrology, v. 56, p. 771–783.

WINTER, B.L., AND KNAUTH, L.P., 1992, Stable isotope geochemistry of carbonate fracture fills in the Monterey Formation, California: Journal of Sedimentary Petrology, v. 62, p. 208–219.

ZENGER, D.H., AND DUNHAM, J.B., 1988, Dolomitization of Siluro–Devonian limestones in a deep core (5,350 m), southeastern New Mexico, *in* Shukla, V., and Baker, P.B., eds., Sedimentology and Geochemistry of Dolostones: SEPM, Special Publication 43, p. 161–173.

Received 20 August 1998; accepted 15 November 2001.